ICCK

Journal of Nonlinear Dynamics and Applications
http://dx.doi.org/10.62762/JNDA.2026.138289

RESEARCH ARTICLE

Global Convergence Regimes of the Return Dynamics in the Class $\mathcal{O}_C$

Mohamed El Morsalani[1,*] **and Mohammed Barkatou**[2]

[1] QWave Consult, Ostfildern, Germany
[2] ISTM Laboratory, Chouaib Doukkali University, El Jadida, Morocco

Abstract

We study the global dynamics of the geometrically generated return map associated with domains in the class $\mathcal{O}_C$. Starting from a convex core $C \subset \mathbb{R}^N$ and a positive thickness function $d : \partial C \to (0,\infty)$, the return construction defines a discrete self-map $F : \partial C \longrightarrow \partial C$ through an outward normal displacement to the outer boundary followed by the inward normal first return to the core. Building on the local geometric theory of the return map, we derive a uniform global one-step estimate $F(c) - c = B_c \nabla_{\partial C} d(c) + O\big(|\nabla_{\partial C} d(c)|^2\big)$, $B_c = d(c)\big(I - d(c)S_c\big)^{-1}$, under explicit smoothness, transversality, and small-slope assumptions. The tangential remainder is shown to be of cubic order. This yields a second-order expansion of the thickness increment governed by the self-adjoint preconditioned Hessian $K_c = B_c^{1/2} H_c B_c^{1/2}$. A directional positivity condition, and in particular the sufficient spectral bound $\lambda_{\min}(K_c) \geq -2 + \delta$, implies strict global thickness ascent, $d(F(c)) - d(c) \geq \gamma |\nabla_{\partial C} d(c)|^2$. Consequently, $\mathcal{V}(c) = d_{\max} - d(c)$ is a strict Lyapunov function. We prove finite Lyapunov dissipation, square summability of the thickness gradient, vanishing return-step size, and, when the critical points of d are isolated, convergence of every orbit to a unique critical point. At nondegenerate attracting maxima we obtain exponential convergence rates from the exact linearization $DF(c_*) = I + B_* H_*$. Within the strict-ascent regime, nontrivial periodic and recurrent orbits are excluded. Finally, numerical computations performed with the exact unit-circle return formula show that the spectral value -2 also marks the local loss of attraction. In a profile for which a multiplier has crossed -1, the exact first-return branch remains globally real, negative thickness increments are detected, and a stable nontrivial period-two orbit is numerically resolved. This provides a concrete exact-map example of the transition from curvature-preconditioned global convergence toward periodic return dynamics.

Keywords: Return map, Gradient-like dynamics, Lyapunov function, Thickness function, Convex core, Class $\mathcal{O}_C$, Discrete dynamical system, Global convergence, Curvature-preconditioned dynamics, Basins of attraction, Period-two orbit.

1 Introduction

A geometric construction can generate a dynamical system without any externally prescribed evolution law. The return map studied in this paper provides a particularly direct instance of this phenomenon.

Submitted: 04 October 2026
Revised: 26 October 2026
Accepted: 17 November 2026
Published: 24 November 2026

Vol. 2, **No.** 4, 2026.
10.62762/JNDA.2026.138289

***Corresponding author:**
✉ Mohamed El Morsalani
mohamed.elmorsalani@qwave-consult.eu

Citation
El Morsalani, M., & Barkatou, M. (2026). Global Convergence Regimes of the Return Dynamics in the Class $\mathcal{O}_C$. *Journal of Nonlinear Dynamics and Applications*, 2(4), 222–260.

© 2026 ICCK (Institute of Central Computation and Knowledge)

A point on the boundary of a convex core is first transported along the outward normal to an enclosing boundary and is then returned to the core by following the inward normal of that outer boundary. Iterating this geometric round trip produces a discrete dynamical system on the boundary of the convex core.

The underlying setting originates in the class $\mathcal{O}_C$ introduced by Barkatou [1]. Let

$$C \subset \mathbb{R}^N$$

be a compact convex body and let

$$d : \partial C \longrightarrow (0, \infty)$$

denote the thickness separating the core from the relevant outer boundary. The radial map is

$$\Phi(c) = c + d(c)\nu(c),$$

where ν is the outward unit normal to ∂C. From $\Phi(c)$ one follows the inward normal of the outer boundary to its first intersection with the convex core. If π denotes this reciprocal first-intersection map, the composition

$$F = \pi \circ \Phi : \partial C \longrightarrow \partial C$$

defines the return dynamics

$$c_{k+1} = F(c_k).$$

The local geometry of this construction was established in [2]. With the sign convention

$$S_c = -D\nu(c)|_{T_c\partial C},$$

the return displacement near a critical point of the thickness satisfies

$$F(c) - c = B_c \nabla_{\partial C} d(c) + O\big(|\nabla_{\partial C} d(c)|^2\big), \qquad (1)$$

where

$$B_c = d(c)\big(I - d(c)S_c\big)^{-1}. \qquad (2)$$

For a convex core the operator B_c is self-adjoint and positive definite. In a principal direction with curvature $\kappa_i(c)$, its eigenvalue is

$$\frac{d(c)}{1 + d(c)\kappa_i(c)}.$$

The leading return displacement is therefore not an ordinary gradient step: the thickness gradient is modified anisotropically by the curvature of the underlying core.

This observation places the return mechanism naturally beside modern developments in geometry-aware optimization. Riemannian formulations of shape optimization interpret shape gradients and shape Hessians through the geometry of spaces of shapes [3, 4], and the geometric-analytic theory of shape derivatives and gradient flows is surveyed in [5]. More generally, optimization constrained to smooth manifolds replaces Euclidean update directions by intrinsic or geometry-dependent directions; recent developments include Riemannian proximal-gradient methods and their global and local convergence theory [6, 7]. The analogy with the present construction is structural rather than algorithmic. Here the preconditioner B_c is not selected to accelerate an optimization procedure. It is forced by the normal geometry of the two boundaries.

Indeed, since B_c is positive definite, one may introduce on $T_c\partial C$ the metric

$$\langle u, v\rangle_{B,c} := \langle B_c^{-1}u, v\rangle. \qquad (3)$$

With respect to this metric, the vector

$$B_c \nabla_{\partial C} d(c)$$

is precisely the Riemannian gradient of the thickness. Thus the return geometry itself generates both a scalar landscape d and the metric that preconditions its leading dynamics. This geometry-induced coupling between landscape, metric, and discrete evolution is one of the motivations for studying the return map globally.

The local theory alone, however, does not determine the behavior of its iterates. In particular, (1) is a local estimate near critical points and does not imply

$$d(F(c)) > d(c)$$

throughout ∂C. Nor does the fact that the leading direction is positive guarantee a global Lyapunov function: a finite discrete step contains second-order and genuinely nonlinear geometric effects. Questions of global monotonicity, orbit convergence, recurrence, and nontrivial periodic dynamics were therefore left open in [2].

The purpose of the present paper is to develop this global theory. The first step is to replace the local expansion (1) by a uniform estimate on the entire compact phase space. Under explicit smoothness, return transversality, and small-slope assumptions, we

prove

$$F(c)-c = B_c\nabla_{\partial C}d(c)+R(c), \qquad |R(c)| \le \Lambda_0|\nabla_{\partial C}d(c)|^2, \tag{4}$$

uniformly in c. More importantly, the tangential component of the remainder is of cubic order. This stronger tangential estimate makes it possible to retain the full second-order information in the variation of the thickness.

Let H_c denote the Riemannian Hessian operator of d and define the self-adjoint preconditioned Hessian

$$K_c = B_c^{1/2}H_cB_c^{1/2}. \tag{5}$$

Writing

$$z_c = B_c^{1/2}\nabla_{\partial C}d(c),$$

we obtain the uniform second-order structure

$$d(F(c)) - d(c) = \left\langle z_c, \left(I + \frac{1}{2}K_c\right) z_c \right\rangle + \mathcal{E}(c), \tag{6}$$

where

$$|\mathcal{E}(c)| \le \eta(|\nabla_{\partial C}d(c)|)\,|\nabla_{\partial C}d(c)|^2, \quad \eta(s) \to 0 \quad (s \downarrow 0).$$

This formula identifies the mechanism by which the local preconditioned-ascent law can lead to global monotonicity.

A natural sufficient condition is the uniform spectral inequality

$$\lambda_{\min}(K_c) \ge -2 + \delta, \qquad \delta > 0, \tag{7}$$

although the global theory is formulated more generally through a directional positivity condition along z_c. Under the resulting ascent assumptions we prove the quantitative inequality

$$d(F(c)) - d(c) \ge \gamma|\nabla_{\partial C}d(c)|^2, \qquad \gamma > 0, \tag{8}$$

away from the fixed-point set. Consequently,

$$\mathcal{V}(c) = d_{\max} - d(c) \tag{9}$$

is a strict Lyapunov function for the return dynamics.

This part of the argument is related in spirit to a broad class of discrete convergence mechanisms in which sufficient decrease, gradient control, and compactness convert a scalar Lyapunov estimate into asymptotic information about the iterates. Such principles appear prominently in modern convergence theory for nonconvex descent methods [8, 9], although the present map differs fundamentally from an algorithmic descent scheme: neither the step nor its preconditioner is chosen externally.

From (8) we obtain the exact telescoping bound

$$\sum_{k=0}^{\infty} |\nabla_{\partial C}d(c_k)|^2 < \infty,$$

and hence

$$|\nabla_{\partial C}d(c_k)| \longrightarrow 0, \qquad |c_{k+1} - c_k| \longrightarrow 0.$$

If the critical points of d are isolated, compactness and the vanishing step size then prevent the orbit from moving indefinitely between distinct critical neighborhoods. Every orbit therefore converges to a unique critical point. No Morse nondegeneracy assumption is needed for this global conclusion.

This distinction is useful in relation to the Kurdyka–Łojasiewicz theory. KL inequalities provide a powerful framework for proving finite-length properties, convergence to single critical points, and quantitative rates for broad classes of gradient and proximal systems [8, 10], including Riemannian proximal-gradient methods [6, 7]. They are not assumed in the main convergence theorem of the present paper. Here isolation of the critical points is sufficient. KL-type hypotheses become relevant instead when one asks how the argument might be extended to nonisolated or degenerate critical sets, a question discussed in Section 10.

The local and global analyses are linked by the same spectral quantity. At a critical point c_*, the exact linearization derived in [2] is

$$DF(c_*) = I + B_*H_*. \tag{10}$$

Since B_*H_* is similar to

$$K_* = B_*^{1/2}H_*B_*^{1/2},$$

if μ_j denotes an eigenvalue of K_*, the corresponding multiplier is

$$\lambda_j = 1 + \mu_j. \tag{11}$$

At a nondegenerate maximum, attraction therefore requires

$$-2 < \mu_j < 0.$$

The value -2 is exactly the point at which a multiplier crosses -1. On the other hand, (6) shows that the same value is the natural spectral boundary at which the full quadratic ascent form

$$I + \frac{1}{2}K_c$$

ceases to be positive definite. Thus the appearance of -2 at both the local and global levels is a geometric consequence of the return construction rather than an independently imposed stability constant.

The unit-circle geometry makes this transition explicit. Because the first-intersection return can be evaluated exactly, the spectral mechanism can be examined without replacing the return map by its first-order approximation. In exact-map examples lying on the $K > -2$ side of the spectral threshold, numerical diagnostics detect no negative thickness increments and show convergence toward attracting maxima. These computations illustrate behavior compatible with the analytical ascent regime, but they are not presented as certified instances of all quantitative hypotheses of Theorem 4.7, in particular the global small-slope threshold. As the relevant preconditioned eigenvalue approaches -2, convergence may become alternating while remaining stable. We then examine a profile for which the multiplier crosses -1 while the exact first-return branch remains globally real. Numerical evaluation of the exact map detects negative thickness increments and resolves a stable nontrivial period-two orbit. These computations provide exact-map evidence that violation of the sufficient convergence regime can produce genuinely different dynamics; they are not used to infer chaotic behavior.

The geometric structure investigated here is also relevant beyond the specific return problem. Normal boundary variations, shape gradients, geometric regularization, and gradient flows are basic tools in shape optimization [3–5]. The present results do not turn the $\mathcal{O}_C$ return map into a general shape optimization algorithm. They instead identify a mechanism that can be relevant whenever repeated normal interactions between nested boundaries generate an effective boundary dynamics: curvature can precondition the motion, alter stability thresholds, and determine whether a scalar geometric quantity remains monotone.

A broader structural analogy also occurs in geometry-aware optimization on nonlinear parameter spaces. Riemannian gradient methods on matrix manifolds, in which the update direction is the gradient taken with respect to the intrinsic metric, are treated systematically in [11] and have been applied to optimization problems of quantum physics and quantum technologies [12]. We do not claim that the present return map models those systems directly; the common principle is only that intrinsic geometry modifies the effective gradient direction and hence the stability of the induced dynamics. Here that modification is generated explicitly by boundary curvature through (2).

The main contributions are:

(1) A uniform one-step estimate for the geometrically defined return map on the whole compact core boundary, together with a cubic tangential remainder under explicit geometric hypotheses (Section 3).

(2) A second-order expansion of the thickness increment in terms of the curvature-preconditioned Hessian K_c, leading to directional and spectral sufficient conditions for strict global ascent (Section 4).

(3) A geometric verification of the strict Lyapunov inequality, from which finite dissipation, gradient square summability, asymptotic regularity and convergence to a unique critical point under isolation follow by standard compactness arguments (Sections 5–6).

(4) A specialization of classical local stability and hyperbolic fixed-point principles to the exact curvature-dependent return-map linearization, including quantitative exponential rates and a classification of convergence classes, attraction basins and recurrence (Sections 7–8).

(5) Exact unit-circle return computations displaying loss of thickness monotonicity and a numerically resolved stable period-two orbit beyond the local multiplier threshold -1 (Section 9).

Items (1)–(2) contain the new analytical ingredients; items (3)–(4) apply standard fixed-point and Lyapunov arguments to them.

The paper is organized as follows. Section 2 recalls only the geometric and local dynamical results from [2] required in the sequel. Section 3 derives the uniform one-step estimate. Section 4 develops the second-order thickness expansion and the global ascent conditions. Section 5 establishes the Lyapunov structure and finite dissipation. Section 6 proves convergence to a unique critical point. Section 7 studies local asymptotics and convergence rates. Section 8 analyzes convergence classes, attraction basins, and recurrence. Section 9 gives the exact unit-circle experiments, including the numerically resolved stable period-two orbit beyond the monotone regime. Finally, Section 10 discusses the scope of the results and several open problems

arising from the boundary between the convergent and nonconvergent regimes.

2 Geometric Framework and Structural Inputs

The return map considered in this paper is the geometrically generated self-map of the convex-core boundary introduced and analyzed in [2]. We recall only the structural ingredients needed for the global analysis and impose explicitly the additional regularity required below. In particular, the local expansion proved in [2] will not be used as a global estimate without further justification.

2.1 Convex core, thickness, and return map

Let

$$C \subset \mathbb{R}^N, \qquad N \geq 2,$$

be a compact convex set with nonempty interior. We assume throughout this paper that

$$\partial C \in C^3.$$

The outward unit normal to ∂C is denoted by

$$\nu : \partial C \longrightarrow \mathbb{S}^{N-1}.$$

We use the sign convention

$$S_c := -D\nu(c)\big|_{T_c\partial C}, \tag{12}$$

for the shape operator of the convex core. Thus, if

$$\kappa_1(c), \ldots, \kappa_{N-1}(c) \geq 0$$

are the usual principal curvatures of the convex hypersurface ∂C, then the eigenvalues of S_c are

$$-\kappa_1(c), \ldots, -\kappa_{N-1}(c).$$

Let Ω belong to the class $\mathcal{O}_C$ considered in [1, 2]. For completeness, we recall the defining geometry in the present smooth-core setting. Write

$$N_\Omega := \{x \in \partial\Omega : n(x) \text{ exists}\}, \ \ell_c := \{c + r\nu(c) : r \in \mathbb{R}\},$$
$$\Delta_c^+ := \{c + r\nu(c) : r \geq 0\}.$$

The C-geometric normal property requires

(P1) $\mathrm{int}(C) \subset \Omega$;

(P2) $\partial\Omega$ is Lipschitz outside C;

(P3) for every $x \in N_\Omega \setminus C$, the inward normal half-line $\{x + tn(x) : t \geq 0\}$ intersects C;

(P4) for every $c \in \partial C$, the set $\ell_c \cap \Omega$ is connected.

The class $\mathcal{O}_C$ consists of such domains for which, in addition, $\partial\Omega \setminus C$ is an orientable $C^{1,1}$ hypersurface, every outward half-normal Δ_c^+ meets $\partial\Omega \setminus C$, and this intersection is transverse. These are precisely the structural assumptions imported from [2]; the stronger C^2 regularity of the thickness and the uniform inward-return transversality used below are additional hypotheses of the present global analysis.

In (P3), t is a free nonnegative parameter describing points along the inward normal ray. In Figure 1, $t(x)$ instead denotes the particular first-hit distance determined by x: namely, $\pi(x) = x + t(x)n(x)$, with $t(x) > 0$ for $x \in \partial\Omega \setminus C$. Thus $t(x)$ is a selected value of the parameter t, not an independent evolution variable.

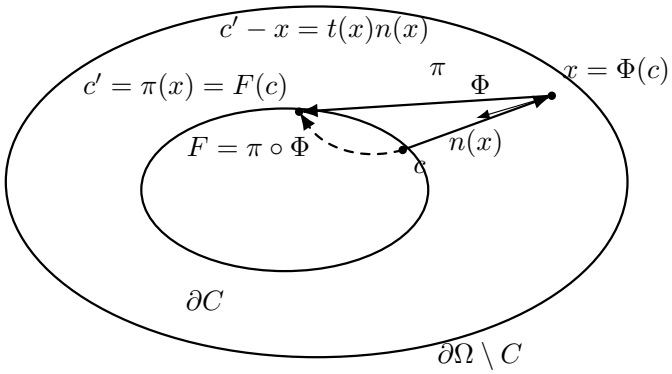

Figure 1. Reciprocal map and return map. Starting from $x = \Phi(c) \in \partial\Omega \setminus C$, the reciprocal map follows the inward normal $n(x)$ to its first intersection $c' = \pi(x) \in \partial C$. The induced return map on the convex core is $F = \pi \circ \Phi$.

The geometric normal property and the radial accessibility result proved in [2] imply that every point $c \in \partial C$ determines a unique point of the outer boundary along the outward normal ray. Hence there exists a positive thickness function

$$d : \partial C \longrightarrow (0, \infty)$$

such that the radial map is

$$\Phi(c) = c + d(c)\nu(c). \tag{13}$$

For the global dynamical analysis we impose the additional regularity assumption

$$d \in C^2(\partial C). \tag{14}$$

Since ∂C is compact, there exist constants

$$0 < d_{\min} \leq d(c) \leq d_{\max} < \infty, \qquad c \in \partial C. \tag{15}$$

Starting from

$$x = \Phi(c) \in \partial\Omega \setminus C,$$

one follows the inward unit normal $n(x)$ to its first intersection with the convex core. Denoting this first-intersection map by

$$\pi : \partial\Omega \setminus C \longrightarrow \partial C,$$

the return map is

$$F = \pi \circ \Phi : \partial C \longrightarrow \partial C. \tag{16}$$

The discrete return dynamics is therefore

$$c_{k+1} = F(c_k), \qquad k \geq 0. \tag{17}$$

In addition to the radial transversality contained in the definition of $\mathcal{O}_C$, we impose the following *uniform inward-return transversality* hypothesis: there exists a constant $\tau_0 > 0$ such that

$$-\big\langle n(\Phi(c)), \nu(F(c))\big\rangle \geq \tau_0, \qquad c \in \partial C. \tag{18}$$

In particular,

$$\big\langle n(\Phi(c)), \nu(F(c))\big\rangle < 0$$

for every $c \in \partial C$. By the reciprocal-map regularity result of [2], this uniform non-tangency implies local regularity of the first-hit branch along $\Phi(\partial C)$; in particular, the induced return map F is continuous on ∂C. The uniform hypothesis prevents tangential first returns and supplies the regularity needed below without deriving it circularly from the continuity of F.

2.2 Exact one-step geometry

We next recall the exact geometric identities established in [2]. Set

$$g_c := \nabla_{\partial C} d(c) \in T_c\partial C \tag{19}$$

and introduce the tangential operator

$$L_c := I - d(c)S_c. \tag{20}$$

By the sign convention (12), the eigenvalues of L_c in the principal directions are

$$1 + d(c)\kappa_i(c) > 0, \qquad i = 1, \dots, N-1. \tag{21}$$

Consequently, L_c is positive definite and invertible for every $c \in \partial C$.

Define

$$w_c := L_c^{-1} g_c = \big(I - d(c)S_c\big)^{-1} \nabla_{\partial C} d(c). \tag{22}$$

The exact inward normal to the outer boundary at the radial point $\Phi(c)$ is

$$n(\Phi(c)) = \frac{-\nu(c) + w_c}{\sqrt{1 + |w_c|^2}}. \tag{23}$$

Let

$$t_c := t(\Phi(c))$$

be the first-return distance from $\Phi(c)$ to the convex core and set

$$\sigma_c := \frac{t_c}{\sqrt{1 + |w_c|^2}}. \tag{24}$$

Then the return displacement admits the exact decomposition

$$F(c) - c = \sigma_c w_c + \big(d(c) - \sigma_c\big)\nu(c). \tag{25}$$

In particular, the metric projection onto the tangent space $T_c\partial C$ is given by

$$P_{T_c\partial C}\big(F(c) - c\big) = \sigma_c w_c, \tag{26}$$

whereas

$$\big\langle F(c) - c, \nu(c)\big\rangle = d(c) - \sigma_c. \tag{27}$$

Equations (23)–(27) are exact. No small-gradient or asymptotic assumption has been used. They will form the starting point for the uniform estimate derived in Section 3.

2.3 The curvature-preconditioning operator

The principal operator governing the local return dynamics is

$$B_c := d(c)L_c^{-1} = d(c)\big(I - d(c)S_c\big)^{-1}. \tag{28}$$

In a principal direction $e_i(c)$ of the convex core,

$$B_c e_i(c) = \frac{d(c)}{1 + d(c)\kappa_i(c)} e_i(c). \tag{29}$$

Thus B_c is self-adjoint and positive definite.

Let

$$\kappa_{\max} := \max_{\substack{c \in \partial C \\ 1 \leq i \leq N-1}} \kappa_i(c). \tag{30}$$

Compactness of ∂C and (15) imply the uniform spectral bounds

$$\beta_- |v|^2 \leq \langle B_c v, v\rangle \leq \beta_+ |v|^2, \qquad v \in T_c\partial C, \tag{31}$$

where one may take

$$\beta_- := \frac{d_{\min}}{1 + d_{\max}\kappa_{\max}}, \qquad \beta_+ := d_{\max}. \tag{32}$$

In particular, the positive direction selected by B_c is uniformly nondegenerate on the compact phase space.

Let

$$H_c : T_c\partial C \longrightarrow T_c\partial C$$

denote the self-adjoint Hessian operator associated with the Riemannian Hessian of d:

$$\langle H_c v, z\rangle = \mathrm{Hess}_{\partial C}\, d(c)[v, z]. \tag{33}$$

We shall repeatedly use the self-adjoint curvature-preconditioned Hessian

$$K_c := B_c^{1/2} H_c B_c^{1/2}. \tag{34}$$

Unlike $B_c H_c$, the operator K_c is self-adjoint, while $B_c H_c$ and K_c are similar and therefore have the same real spectrum.

This operator will play two related roles below. Locally, at a critical point, its eigenvalues determine the multipliers of the linearized return map. Globally, it will enter the second-order variation of the thickness along one return step.

2.4 Fixed points and local linearization

The foundational analysis in [2] identifies the equilibria of the return dynamics with the critical points of the thickness function. Under the present smoothness assumptions this holds pointwise:

$$F(c) = c \quad \Longleftrightarrow \quad \nabla_{\partial C} d(c) = 0. \tag{35}$$

Let $c_* \in \partial C$ be a critical point and write

$$d_* := d(c_*),\ B_* := d_*\big(I - d_* S_*\big)^{-1},\ H_* := H_{c_*}. \tag{36}$$

The exact derivative of the return map at c_* is

$$DF(c_*)\big|_{T_{c_*}\partial C} = I + B_* H_*. \tag{37}$$

If

$$\mu_1, \dots, \mu_{N-1}$$

are the eigenvalues of

$$K_* = B_*^{1/2} H_* B_*^{1/2},$$

then the multipliers of the return map are

$$\lambda_j = 1 + \mu_j, \qquad j = 1, \dots, N-1. \tag{38}$$

In particular, the threshold

$$-2 < \mu_j < 0 \tag{39}$$

characterizes linear attraction at a nondegenerate local maximum. Nondegenerate minima are repelling, while a nondegenerate saddle has at least one unstable direction. These local facts will serve as a consistency requirement for the global theory developed below.

2.5 Local versus global control

A central point for the present paper is the distinction between the local result already available and the global estimate that remains to be proved.

Near a critical point, [2] establishes the quadratic remainder estimate

$$\begin{aligned} F(c) - c &= B_c \nabla_{\partial C} d(c) + R(c), \\ |R(c)| &\le \Lambda |\nabla_{\partial C} d(c)|^2, \end{aligned} \tag{40}$$

for c in a sufficiently small local-return neighborhood. Hence the leading displacement points in a curvature-preconditioned gradient-ascent direction.

Estimate (40), however, is a *local* statement. It does not imply that

$$d(F(c)) > d(c) \tag{41}$$

for every noncritical point of ∂C, nor does it provide a uniform quadratic remainder bound on the whole phase space.

Accordingly, we shall not assume (40) globally. The next section derives a uniform one-step estimate directly from the exact geometry (25), under explicit global small-slope and local-return hypotheses. That estimate will provide the bridge from the local theory of [2] to the Lyapunov and convergence results of the present paper.

3 Uniform Global Control of One Return Step

The quadratic remainder estimate established in [2] is local: it is proved in a sufficiently small return neighborhood of a critical point of the thickness function. For the global convergence analysis developed below, this local statement must be replaced by a uniform estimate valid on the whole compact phase space.

The purpose of this section is to derive such an estimate directly from the exact return geometry recalled in Section 2. The essential ingredients are the compactness of ∂C, uniform local graph representations of the convex core, global return transversality, and a uniform small-slope condition.

3.1 Uniform normal-graph geometry of the convex core

We begin with a uniform version of the local normal-graph representation of ∂C.

Lemma 3.1 (Uniform normal-graph representation)**.** *There exist constants*

$$\rho_0 > 0, \qquad r_0 > 0, \qquad K_C > 0,$$

such that for every $c \in \partial C$, the portion of ∂C contained in $B_{\rho_0}(c)$ can be represented uniquely in the form

$$u \longmapsto c + u + h_c(u)\nu(c), \qquad u \in B_{r_0}^{T_c\partial C}(0), \tag{42}$$

where

$$h_c(0) = 0, \qquad Dh_c(0) = 0, \tag{43}$$

and

$$|h_c(u)| \le K_C|u|^2. \tag{44}$$

Moreover, convexity implies

$$h_c(u) \le 0. \tag{45}$$

The constants ρ_0, r_0, and K_C may be chosen independently of c.

Proof. Since ∂C is a compact C^3 hypersurface, every $c \in \partial C$ admits a local representation as a graph over its tangent space. The C^2 norms of these local graph functions can be chosen uniformly after passing to a finite covering of ∂C. This yields uniform constants ρ_0, r_0, and K_C such that (42)–(44) hold.

To obtain the sign, observe that the tangent hyperplane at c is a supporting hyperplane of the convex set C. Hence every nearby point

$$q = c + u + h_c(u)\nu(c) \in \partial C$$

satisfies

$$\langle q - c, \nu(c)\rangle = h_c(u) \le 0,$$

which proves (45). □

3.2 Uniform control of the return distance

Recall that

$$t_c := t(\Phi(c))$$

denotes the first-return distance from the outer boundary to the convex core and

$$\sigma_c = \frac{t_c}{\sqrt{1 + |w_c|^2}}.$$

Lemma 3.2 (Uniform boundedness of the return parameter)**.** *There exists a constant $T_0 < \infty$ such that*

$$0 < t_c \le T_0, \qquad 0 < \sigma_c \le T_0, \qquad c \in \partial C. \tag{46}$$

One may take

$$T_0 := d_{\max} + \operatorname{diam}(C). \tag{47}$$

Proof. Since $F(c) \in \partial C$ and $\Phi(c) = c + d(c)\nu(c)$,

$$\begin{aligned} t_c = |\Phi(c) - F(c)| &\le |\Phi(c) - c| + |c - F(c)| \\ &\le d_{\max} + \operatorname{diam}(C). \end{aligned}$$

This gives the asserted bound for t_c. The estimate for σ_c follows from

$$\sigma_c = \frac{t_c}{\sqrt{1 + |w_c|^2}} \le t_c.$$

□

The next lemma is the step that allows the local graph geometry of Lemma 3.1 to be used uniformly.

Lemma 3.3 (Small slope implies uniform local return)**.** *There exists a constant*

$$\varepsilon_{\mathrm{lr}} > 0$$

such that

$$|w_c| \le \varepsilon_{\mathrm{lr}} \tag{48}$$

implies

$$|F(c) - c| < \rho_0. \tag{49}$$

Here ρ_0 is the uniform graph radius from Lemma 3.1.

Proof. Suppose that the assertion were false. Then there would exist a sequence $(c_j) \subset \partial C$ such that

$$|w_{c_j}| \longrightarrow 0, \qquad |F(c_j) - c_j| \ge \rho_0. \tag{50}$$

By compactness, after passing to a subsequence,

$$c_j \longrightarrow c_* \in \partial C.$$

The map

$$c \longmapsto w_c = \big(I - d(c)S_c\big)^{-1}\nabla_{\partial C} d(c)$$

is continuous under the standing regularity assumptions. Hence

$$w_{c_*} = 0.$$

Since $I - d(c_*)S_{c_*}$ is invertible, this is equivalent to

$$\nabla_{\partial C} d(c_*) = 0.$$

The fixed-point characterization established in [2] therefore gives

$$F(c_*) = c_*.$$

By the continuity of F stated after (18),

$$F(c_j) - c_j \longrightarrow F(c_*) - c_* = 0,$$

contradicting (50). □

Remark 3.4. Since the eigenvalues of

$$L_c = I - d(c)S_c$$

are at least 1, one has

$$\|L_c^{-1}\| \le 1.$$

Therefore

$$|w_c| \le |\nabla_{\partial C} d(c)|. \tag{51}$$

Thus the stronger but simpler condition

$$\|\nabla_{\partial C} d\|_{L^\infty(\partial C)} \le \varepsilon_{\mathrm{lr}}$$

is sufficient for the uniform local-return property.

3.3 Uniform quadratic remainder estimate

Set

$$L_{\max} := 1 + d_{\max}\kappa_{\max}. \tag{52}$$

Since the eigenvalues of $L_c = I - d(c)S_c$ belong to $[1, L_{\max}]$, one has

$$|\nabla_{\partial C} d(c)| \le L_{\max}|w_c|.$$

We now impose the global small-slope condition

$$\begin{aligned} &\|w\|_{L^\infty(\partial C)} \le \varepsilon_0, \\ &0 < \varepsilon_0 \le \min\left\{1,\ \varepsilon_{\mathrm{lr}},\ \frac{r_0}{2T_0 L_{\max}}\right\}. \end{aligned} \tag{53}$$

The last restriction guarantees

$$T_0|\nabla_{\partial C} d(c)| \le \frac{r_0}{2} < r_0 \qquad \text{for every } c \in \partial C, \tag{54}$$

which will keep the Taylor remainder of Section 4.1 inside the uniform normal-graph chart.

Under this condition, every return point $F(c)$ lies in the uniform normal-graph neighborhood of its starting point c.

Theorem 3.5 (Uniform global one-step estimate)**.** *Assume* (53)*. Then there exists a constant* $\Lambda_0 > 0$*, independent of* c*, such that for every* $c \in \partial C$*,*

$$F(c) - c = B_c \nabla_{\partial C} d(c) + R(c), \tag{55}$$

where

$$|R(c)| \le \Lambda_0 |\nabla_{\partial C} d(c)|^2. \tag{56}$$

More precisely,

$$0 \le \sigma_c - d(c) \le K_C T_0^2 |w_c|^2, \tag{57}$$

and the tangential component satisfies the stronger estimate

$$P_{T_c\partial C}\big(F(c) - c\big) = B_c \nabla_{\partial C} d(c) + R_T(c), \tag{58}$$

with

$$|R_T(c)| \le K_C T_0^2 |w_c|^3. \tag{59}$$

Proof. Fix $c \in \partial C$. By Lemma 3.3 and (53), the point $F(c)$ belongs to the uniform normal-graph neighborhood based at c. Hence there exists a unique $u_c \in T_c\partial C$ such that

$$F(c) - c = u_c + h_c(u_c)\nu(c). \tag{60}$$

On the other hand, the exact return decomposition recalled in (25) gives

$$F(c) - c = \sigma_c w_c + \big(d(c) - \sigma_c\big)\nu(c).$$

Comparing tangent and normal components yields

$$u_c = \sigma_c w_c \tag{61}$$

and

$$d(c) - \sigma_c = h_c(\sigma_c w_c). \tag{62}$$

By convexity,

$$h_c(\sigma_c w_c) \le 0,$$

so

$$\sigma_c \ge d(c).$$

Furthermore, using (44) and (46),

$$0 \le \sigma_c - d(c) \le K_C \sigma_c^2 |w_c|^2 \le K_C T_0^2 |w_c|^2,$$

which proves (57).

We now subtract the leading tangential term $d(c)w_c$ from the exact return displacement:

$$\begin{aligned} F(c) - c - d(c)w_c &= (\sigma_c - d(c))w_c + (d(c) - \sigma_c)\nu(c) \\ &= (\sigma_c - d(c))\big(w_c - \nu(c)\big). \end{aligned} \tag{63}$$

Therefore,

$$\begin{aligned} |F(c) - c - d(c)w_c| &= |\sigma_c - d(c)|\sqrt{1 + |w_c|^2} \\ &\le K_C T_0^2 \sqrt{1 + \varepsilon_0^2}\,|w_c|^2. \end{aligned} \tag{64}$$

Since $\varepsilon_0 \le 1$, one may take

$$\Lambda_0 = \Lambda_w = \sqrt{2}\, K_C T_0^2.$$

Finally,

$$d(c)w_c = d(c)\big(I - d(c)S_c\big)^{-1}\nabla_{\partial C} d(c) = B_c \nabla_{\partial C} d(c),$$

and (51) gives

$$|w_c| \le |\nabla_{\partial C} d(c)|.$$

Thus

$$|R(c)| \le \Lambda_w |\nabla_{\partial C} d(c)|^2,$$

which proves (55)–(56).

For the tangential component,

$$P_{T_c\partial C}(F(c)-c)=\sigma_c w_c.$$

Hence

$$R_T(c)=(\sigma_c-d(c))w_c,$$

and (57) gives

$$|R_T(c)|\le K_C T_0^2|w_c|^3.$$

This proves (58) and (59). □

3.4 Gradient-step comparability

The preceding theorem gives several uniform estimates that will be used repeatedly in the global convergence argument.

Recall from (52) that

$$L_{\max}=1+d_{\max}\kappa_{\max}.$$

Since the eigenvalues of L_c belong to $[1,L_{\max}]$, the eigenvalues of L_c^{-1} belong to $[L_{\max}^{-1},1]$. Therefore

$$\frac{1}{L_{\max}}|\nabla_{\partial C}d(c)|\le|w_c|\le|\nabla_{\partial C}d(c)|. \tag{65}$$

Corollary 3.6 (Uniform control of one-step displacement)**.** *Under the assumptions of Theorem 3.5, there exists a constant $C_F>0$ such that*

$$|F(c)-c|\le C_F|\nabla_{\partial C}d(c)| \tag{66}$$

for every $c\in\partial C$.

Moreover, the tangential displacement satisfies

$$\beta_-|\nabla_{\partial C}d(c)|\le|P_{T_c\partial C}(F(c)-c)|\le T_0|\nabla_{\partial C}d(c)|, \tag{67}$$

where

$$\beta_-=\frac{d_{\min}}{1+d_{\max}\kappa_{\max}}>0. \tag{68}$$

Proof. From Theorem 3.5,

$$|F(c)-c|\le d_{\max}|w_c|+\Lambda_w|w_c|^2.$$

Since $|w_c|\le\varepsilon_0$,

$$|F(c)-c|\le\big(d_{\max}+\Lambda_w\varepsilon_0\big)|w_c|.$$

Using (51) proves (66).

For the tangential component,

$$|P_{T_c\partial C}(F(c)-c)|=\sigma_c|w_c|.$$

Since

$$d(c)\le\sigma_c\le T_0,$$

and by (65),

$$\sigma_c|w_c|\ge d_{\min}\frac{1}{L_{\max}}|\nabla_{\partial C}d(c)|=\beta_-|\nabla_{\partial C}d(c)|.$$

The upper bound follows from

$$\sigma_c|w_c|\le T_0|\nabla_{\partial C}d(c)|.$$

□

Remark 3.7. Theorem 3.5 is not a restatement of the local expansion proved in [2]. The new content is the uniformity over the entire compact phase space ∂C, obtained from the global transversality and small-slope assumptions.

A further feature of the proof is the distinction between the full ambient remainder and its tangential component:

$$R(c)=O(|\nabla_{\partial C}d(c)|^2),$$

whereas

$$R_T(c)=O(|\nabla_{\partial C}d(c)|^3).$$

The latter estimate will be important in the second-order expansion of the thickness increment in the next section.

Remark 3.8 (Role of the small-slope hypothesis). The small-slope condition is a sufficient geometric hypothesis used to place every first return inside a uniform normal-graph neighborhood and thereby obtain the uniform quadratic one-step estimate. No necessity is claimed. In particular, the exact return map may remain globally well defined outside this perturbative regime, as the unit-circle computations of Section 9 illustrate.

4 Curvature-Preconditioned Ascent

The uniform one-step estimate of Section 3 shows that the tangential part of the return displacement is, to leading order,

$$B_c\nabla_{\partial C}d(c),$$

where

$$B_c=d(c)\big(I-d(c)S_c\big)^{-1}.$$

Since B_c is positive definite, this leading displacement points in a direction of increasing thickness. The purpose of the present section is to determine conditions under which this local tendency produces a

one-step increase of the thickness on the whole phase space.

The second-order term is essential. It introduces the curvature-preconditioned Hessian

$$K_c = B_c^{1/2} H_c B_c^{1/2},$$

and leads naturally to the same spectral threshold -2 that appears in the local stability theory of the return map.

4.1 Uniform second-order expansion of the thickness

For $c \in \partial C$, let

$$\Psi_c(u) = c + u + h_c(u)\nu(c)$$

be the uniform normal-graph parametrization supplied by Lemma 3.1. Define

$$\widetilde{d}_c(u) := d(\Psi_c(u)). \tag{69}$$

The following uniform Taylor formula will be used throughout this section.

Lemma 4.1 (Uniform second-order Taylor formula). *There exists a nondecreasing function*

$$\omega_d : [0, r_0] \longrightarrow [0, \infty)$$

with

$$\omega_d(r) \longrightarrow 0 \qquad \text{as } r \downarrow 0, \tag{70}$$

such that, for every $c \in \partial C$ and every $u \in T_c\partial C$ with $|u| < r_0$,

$$d(\Psi_c(u)) - d(c) = \langle g_c, u\rangle + \frac{1}{2}\langle H_c u, u\rangle + \mathcal{T}_c(u), \tag{71}$$

where

$$|\mathcal{T}_c(u)| \le \frac{1}{2}\omega_d(|u|)|u|^2. \tag{72}$$

Here

$$g_c = \nabla_{\partial C} d(c)$$

and H_c is the Hessian operator defined in (33).

Proof. At $u = 0$,

$$D\Psi_c(0) = I$$

on $T_c\partial C$. Hence

$$D\widetilde{d}_c(0)[u] = \langle g_c, u\rangle.$$

Moreover,

$$D^2\Psi_c(0)[u, v] = D^2 h_c(0)[u, v]\nu(c)$$

is normal to $T_c\partial C$. Thus the Christoffel symbols of the coordinates induced by Ψ_c vanish at the origin. Consequently, the ordinary Hessian of $\widetilde{d}_c$ at $u = 0$ coincides with the intrinsic Hessian of d:

$$D^2\widetilde{d}_c(0)[u, v] = \mathrm{Hess}_{\partial C}\, d(c)[u, v] = \langle H_c u, v\rangle. \tag{73}$$

Since $d \in C^2(\partial C)$ and ∂C is compact, choose a finite atlas of the uniform normal-graph neighborhoods above. In this atlas the graph parametrizations depend C^2-continuously on the base point c. Consequently, on the associated compact closed disk bundle, the map

$$(c, u) \longmapsto D^2(d \circ \Psi_c)(u)$$

is uniformly continuous. Hence the second derivatives of the pulled-back functions $\widetilde{d}_c$ admit a single modulus of continuity independent of c. Therefore there exists a modulus ω_d satisfying (70) such that

$$\left\| D^2\widetilde{d}_c(v) - D^2\widetilde{d}_c(0) \right\| \le \omega_d(|u|)$$

whenever $|v| \le |u| < r_0$.

Taylor's formula with integral remainder then yields (71) and (72). □

4.2 Second-order variation along one return step

We now apply Lemma 4.1 to the return point $F(c)$.

Let

$$u_c := P_{T_c\partial C}\big(F(c) - c\big). \tag{74}$$

By Theorem 3.5,

$$u_c = B_c g_c + r_c, \tag{75}$$

where

$$|r_c| \le C_T |g_c|^3, \qquad C_T := K_C T_0^2. \tag{76}$$

Moreover,

$$|u_c| = \sigma_c |w_c| \le T_0 |g_c|. \tag{77}$$

By (54),

$$T_0|g_c| < r_0,$$

so every occurrence of $\omega_d(T_0|g_c|)$ below lies inside the domain of the modulus introduced in Lemma 4.1.

Define

$$z_c := B_c^{1/2} g_c. \tag{78}$$

Theorem 4.2 (Second-order thickness increment). *Under the assumptions of Theorem 3.5, one has*

$$d(F(c)) - d(c) = \left\langle z_c, \left(I + \frac{1}{2}K_c\right) z_c \right\rangle + \mathcal{E}(c), \tag{79}$$

where

$$K_c = B_c^{1/2} H_c B_c^{1/2},$$

and the remainder satisfies

$$|\mathcal{E}(c)| \le \eta(|g_c|)|g_c|^2. \tag{80}$$

Here $\eta : [0, L_{\max}\varepsilon_0] \to [0, \infty)$ *may be chosen so that*

$$\eta(s) \longrightarrow 0 \qquad \text{as } s \downarrow 0. \tag{81}$$

More explicitly, one may take

$$\eta(s) = C_T s^2 + M_H d_{\max} C_T s^2 + \frac{1}{2} M_H C_T^2 s^4 + \frac{1}{2} T_0^2 \omega_d(T_0 s), \tag{82}$$

where

$$M_H := \max_{c \in \partial C} \|H_c\|. \tag{83}$$

Proof. Since

$$F(c) = \Psi_c(u_c),$$

Lemma 4.1 gives

$$d(F(c)) - d(c) = \langle g_c, u_c \rangle + \frac{1}{2}\langle H_c u_c, u_c \rangle + \mathcal{T}_c(u_c). \tag{84}$$

Set

$$q_c := B_c g_c.$$

Then

$$u_c = q_c + r_c.$$

For the linear term,

$$\begin{aligned} \langle g_c, u_c \rangle &= \langle g_c, B_c g_c \rangle + \langle g_c, r_c \rangle \\ &= |z_c|^2 + \langle g_c, r_c \rangle, \end{aligned} \tag{85}$$

because

$$|z_c|^2 = \langle g_c, B_c g_c \rangle.$$

Furthermore,

$$|\langle g_c, r_c \rangle| \le C_T |g_c|^4. \tag{86}$$

For the quadratic term,

$$\langle H_c u_c, u_c \rangle = \langle H_c q_c, q_c \rangle + 2\langle H_c q_c, r_c \rangle + \langle H_c r_c, r_c \rangle. \tag{87}$$

Since

$$q_c = B_c g_c = B_c^{1/2} z_c,$$

one obtains

$$\begin{aligned} \langle H_c q_c, q_c \rangle &= \left\langle H_c B_c^{1/2} z_c, B_c^{1/2} z_c \right\rangle \\ &= \langle K_c z_c, z_c \rangle. \end{aligned} \tag{88}$$

Using

$$\|B_c\| \le d_{\max}$$

and (76),

$$|\langle H_c q_c, r_c \rangle| \le M_H d_{\max} C_T |g_c|^4, \tag{89}$$

$$|\langle H_c r_c, r_c \rangle| \le M_H C_T^2 |g_c|^6. \tag{90}$$

Finally, by (77) and (72),

$$\begin{aligned} |\mathcal{T}_c(u_c)| &\le \frac{1}{2}\omega_d(|u_c|)|u_c|^2 \\ &\le \frac{1}{2} T_0^2 \omega_d(T_0|g_c|)|g_c|^2. \end{aligned} \tag{91}$$

Substituting (85)–(91) into (84) gives (79). Collecting the remainder terms yields (80) with (82). Since

$$\omega_d(r) \to 0 \qquad \text{as } r \to 0,$$

one has $\eta(s) \to 0$ as $s \to 0$. □

Remark 4.3. Formula (79) identifies the two contributions governing one return step:

$$|z_c|^2$$

is the positive first-order ascent term, whereas

$$\frac{1}{2}\langle K_c z_c, z_c \rangle$$

is the second-order correction induced jointly by the Hessian of the thickness and the curvature-dependent preconditioner B_c.

4.3 A uniform ascent condition

The preceding theorem suggests the following condition.

Definition 4.4 (Uniform preconditioned-ascent condition)**.** We say that the thickness landscape satisfies the uniform preconditioned-ascent condition if there exists a constant $\alpha_0 > 0$ such that

$$\left\langle z_c, \left(I + \frac{1}{2}K_c\right) z_c \right\rangle \ge \alpha_0 |z_c|^2 \tag{92}$$

for every $c \in \partial C$.

Condition (92) is directional: it requires positivity only in the dynamically relevant direction

$$z_c = B_c^{1/2}\nabla_{\partial C} d(c).$$

A stronger but simpler spectral condition gives an immediate sufficient criterion.

Proposition 4.5 (Spectral sufficient condition). *Assume that there exists $\delta > 0$ such that*

$$\lambda_{\min}(K_c) \geq -2 + \delta \qquad \text{for every } c \in \partial C. \tag{93}$$

Then the uniform preconditioned-ascent condition holds with

$$\alpha_0 = \frac{\delta}{2}. \tag{94}$$

Proof. Condition (93) implies

$$K_c \geq (-2+\delta)I$$

in the sense of quadratic forms. Therefore

$$I + \frac{1}{2}K_c \geq \frac{\delta}{2} I.$$

Hence

$$\left\langle z_c, \left(I + \frac{1}{2}K_c\right) z_c \right\rangle \geq \frac{\delta}{2}|z_c|^2,$$

which proves the assertion. □

Remark 4.6. The directional condition (92) is weaker than the uniform spectral condition (93). The global convergence theory below therefore does not require every direction of K_c to satisfy the bound $-2+\delta$; it is enough that the quadratic form be uniformly positive along the preconditioned gradient direction.

The spectral condition is nevertheless geometrically transparent and will be useful for comparison with the local stability threshold. It controls directions that may never be sampled by the return dynamics and is therefore generally stronger than necessary. In particular, $\lambda_{\min}(K_c) < -2$ at some point does not by itself imply loss of thickness monotonicity, because the corresponding eigendirection may be poorly aligned with z_c.

4.4 Strict global increase of the thickness

Recall the uniform coercivity estimate

$$|z_c|^2 = \langle B_c g_c, g_c\rangle \geq \beta_- |g_c|^2, \tag{95}$$

where

$$\beta_- = \frac{d_{\min}}{1 + d_{\max}\kappa_{\max}} > 0.$$

Also recall from (65) that

$$|g_c| \leq L_{\max}|w_c|, \qquad L_{\max} = 1 + d_{\max}\kappa_{\max}. \tag{96}$$

Theorem 4.7 (Uniform strict ascent). *Assume the uniform preconditioned-ascent condition (92). Then there exists*

$$\varepsilon_{\text{asc}} > 0$$

such that, if

$$\|w\|_{L^\infty(\partial C)} \leq \varepsilon_{\text{asc}}, \tag{97}$$

the return map satisfies

$$d(F(c)) - d(c) \geq \gamma |\nabla_{\partial C} d(c)|^2 \tag{98}$$

for every $c \in \partial C$, where

$$\gamma := \frac{\alpha_0 \beta_-}{2} > 0. \tag{99}$$

Consequently,

$$d(F(c)) \geq d(c) \tag{100}$$

for every $c \in \partial C$, with equality if and only if

$$\nabla_{\partial C} d(c) = 0, \tag{101}$$

or equivalently,

$$F(c) = c. \tag{102}$$

Proof. By Theorem 4.2,

$$d(F(c)) - d(c) = \left\langle z_c, \left(I + \frac{1}{2}K_c\right) z_c \right\rangle + \mathcal{E}(c). \tag{103}$$

The ascent condition gives

$$\left\langle z_c, \left(I + \frac{1}{2}K_c\right) z_c \right\rangle \geq \alpha_0 |z_c|^2 \geq \alpha_0 \beta_- |g_c|^2.$$

Hence

$$d(F(c)) - d(c) \geq (\alpha_0\beta_- - \eta(|g_c|))\,|g_c|^2. \tag{104}$$

Since $\eta(s) \to 0$ as $s \downarrow 0$, choose $s_{\text{asc}} > 0$ so that

$$\eta(s) \leq \frac{\alpha_0\beta_-}{2} \qquad \text{for } 0 \leq s \leq s_{\text{asc}}. \tag{105}$$

Now choose

$$\varepsilon_{\text{asc}} \leq \min\left\{\varepsilon_0, \frac{s_{\text{asc}}}{L_{\max}}\right\}. \tag{106}$$

Then (96) gives

$$|g_c| \leq s_{\text{asc}}$$

for every c, so (104) becomes

$$d(F(c)) - d(c) \geq \frac{\alpha_0\beta_-}{2}|g_c|^2.$$

This proves (98).

If $g_c \neq 0$, the right-hand side is strictly positive. If $g_c = 0$, the fixed-point characterization from [2] gives $F(c) = c$, so equality holds. This proves the final assertions. □

The threshold $\varepsilon_{\mathrm{asc}}$ is quantitative once the uniform graph constants and a modulus of continuity for the Hessian are specified: one first chooses s_{asc} from (105) and then uses (106). No universal closed-form value is expected under the present C^2 assumptions, because the admissible threshold depends on these geometric and continuity data.

Under the spectral condition (93), one may take

$$\alpha_0 = \frac{\delta}{2},$$

and hence

$$\gamma = \frac{\delta\beta_-}{4}. \tag{107}$$

4.5 Two-sided control of the thickness increment

For later use we also record an upper bound.

Since K_c depends continuously on c and ∂C is compact, set

$$M_K := \max_{c\in\partial C} \|K_c\|. \tag{108}$$

Corollary 4.8 (Quadratic comparability of the thickness increment)**.** *Under the assumptions of Theorem 4.7, there exists a constant $\Gamma > 0$ such that*

$$\gamma|\nabla_{\partial C} d(c)|^2 \le d(F(c)) - d(c) \le \Gamma|\nabla_{\partial C} d(c)|^2 \tag{109}$$

for every $c \in \partial C$.

Proof. The lower bound is (98).

For the upper bound, use

$$|z_c|^2 \le \beta_+ |g_c|^2, \qquad \beta_+ = d_{\max},$$

and

$$\left|\left\langle z_c, \left(I + \frac{1}{2}K_c\right) z_c \right\rangle\right| \le \left(1 + \frac{1}{2}M_K\right)|z_c|^2.$$

The remainder estimate (80) then gives

$$d(F(c)) - d(c) \le \left[\beta_+\left(1 + \frac{1}{2}M_K\right) + \eta(s_{\mathrm{asc}})\right]|g_c|^2.$$

Thus one may take

$$\Gamma = \beta_+\left(1 + \frac{1}{2}M_K\right) + \eta(s_{\mathrm{asc}}). \tag{110}$$

□

4.6 Relation with the local stability threshold

The spectral condition

$$\lambda_{\min}(K_c) > -2$$

is not introduced arbitrarily. The same threshold occurs in the exact local linearization established in [2].

At a critical point c_*,

$$DF(c_*) = I + B_* H_*,$$

and $B_* H_*$ is similar to the self-adjoint operator

$$K_* = B_*^{1/2} H_* B_*^{1/2}.$$

If μ_j are the eigenvalues of K_*, the multipliers of the return map are

$$\lambda_j = 1 + \mu_j.$$

Consequently, a nondegenerate local maximum is linearly attracting precisely when

$$-2 < \mu_j < 0$$

for every j.

The global condition (93) controls the lower part of this same spectral range uniformly over ∂C. It prevents the second-order curvature–Hessian contribution from overwhelming the positive first-order ascent term.

The role of the threshold is therefore consistent at both scales: locally it prevents an attracting maximum from overshooting through a multiplier of modulus at least one, while globally it provides a natural sufficient condition for strict increase of the thickness after one return step.

We emphasize that (93) is a sufficient global condition, not a necessary characterization of all geometries for which the thickness is monotone.

5 Lyapunov Structure of the Return Dynamics

Throughout this section we assume the hypotheses of Theorem 4.7. In particular, there exist constants

$$0 < \gamma \le \Gamma < \infty$$

such that

$$\gamma|\nabla_{\partial C} d(c)|^2 \le d(F(c)) - d(c) \le \Gamma|\nabla_{\partial C} d(c)|^2 \tag{111}$$

for every $c \in \partial C$.

Since $d \in C^2(\partial C)$ and ∂C is compact, we set

$$d_{\max} := \max_{c\in\partial C} d(c). \tag{112}$$

5.1 Thickness deficit as a Lyapunov function

The return dynamics moves, under the assumptions of the preceding section, in the direction of increasing thickness. It is therefore natural to measure the remaining thickness deficit from the global maximum.

Definition 5.1 (Thickness-deficit Lyapunov function)**.** Define

$$\mathcal{V}(c) := d_{\max} - d(c), \qquad c \in \partial C. \tag{113}$$

Then

$$\mathcal{V}(c) \geq 0$$

on ∂C.

For later use, define also the one-step thickness gain

$$\mathcal{D}(c) := d(F(c)) - d(c). \tag{114}$$

Although $\mathcal{D}$ measures an increase of the thickness, it is the exact dissipation of the deficit $\mathcal{V}$:

$$\mathcal{V}(c) - \mathcal{V}(F(c)) = \mathcal{D}(c). \tag{115}$$

Theorem 5.2 (Strict Lyapunov inequality)**.** *For every $c \in \partial C$,*

$$\gamma|\nabla_{\partial C} d(c)|^2 \leq \mathcal{V}(c) - \mathcal{V}(F(c)) \leq \Gamma|\nabla_{\partial C} d(c)|^2. \tag{116}$$

Equivalently,

$$-\Gamma|\nabla_{\partial C} d(c)|^2 \leq \mathcal{V}(F(c)) - \mathcal{V}(c) \leq -\gamma|\nabla_{\partial C} d(c)|^2. \tag{117}$$

Consequently,

$$\mathcal{V}(F(c)) \leq \mathcal{V}(c), \tag{118}$$

with equality if and only if

$$\nabla_{\partial C} d(c) = 0. \tag{119}$$

Under the fixed-point characterization recalled in Section 2.4, this is equivalent to

$$F(c) = c. \tag{120}$$

Proof. By definition,

$$\mathcal{V}(c) - \mathcal{V}(F(c)) = d(F(c)) - d(c).$$

The two-sided estimate (116) is therefore exactly (111).

If $\nabla_{\partial C} d(c) \neq 0$, the lower bound gives

$$\mathcal{V}(F(c)) < \mathcal{V}(c).$$

If $\nabla_{\partial C} d(c) = 0$, then c is a fixed point of F, and equality follows. □

Remark 5.3. The function $\mathcal{V}$ is a strict Lyapunov function relative to the fixed-point set of the return map. Its zero set consists of the global maxima of d, whereas its one-step variation vanishes at every critical point of d, because every such point is an exact fixed point of F. Thus no claim is made that all equilibria minimize $\mathcal{V}$.

5.2 Monotonicity along return orbits

Let

$$c_{k+1} = F(c_k), \qquad k \geq 0, \tag{121}$$

be an arbitrary return orbit, and write

$$d_k := d(c_k), \quad \mathcal{V}_k := \mathcal{V}(c_k), \quad g_k := \nabla_{\partial C} d(c_k). \tag{122}$$

The strict ascent theorem gives

$$d_{k+1} - d_k \geq \gamma|g_k|^2 \geq 0. \tag{123}$$

Hence (d_k) is nondecreasing. Since

$$d_k \leq d_{\max},$$

there exists

$$d_\infty \in [d(c_0), d_{\max}] \tag{124}$$

such that

$$d_k \longrightarrow d_\infty. \tag{125}$$

Equivalently,

$$\mathcal{V}_k \longrightarrow \mathcal{V}_\infty := d_{\max} - d_\infty. \tag{126}$$

At this stage, the existence of the scalar limit d_∞ does not yet imply convergence of the orbit (c_k) itself. Establishing that stronger conclusion is the subject of Section 6.

5.3 Exact telescoping balance and finite dissipation

The Lyapunov identity telescopes exactly along every orbit.

Proposition 5.4 (Finite Lyapunov dissipation)**.** *For every integer $n \geq 1$,*

$$\mathcal{V}(c_n) + \sum_{k=0}^{n-1} \mathcal{D}(c_k) = \mathcal{V}(c_0). \tag{127}$$

Consequently,

$$\sum_{k=0}^{\infty} \mathcal{D}(c_k) = \mathcal{V}(c_0) - \mathcal{V}_\infty = d_\infty - d(c_0) < \infty. \tag{128}$$

Proof. Equation (115) gives

$$\mathcal{D}(c_k) = \mathcal{V}(c_k) - \mathcal{V}(c_{k+1}).$$

Summing from $k = 0$ to $n - 1$ gives

$$\sum_{k=0}^{n-1} \mathcal{D}(c_k) = \mathcal{V}(c_0) - \mathcal{V}(c_n),$$

which is equivalent to (127).

Passing to the limit $n \to \infty$ and using (126) yields (128). □

Thus the total increase of the thickness along an orbit is finite, even though the orbit may contain infinitely many nontrivial return steps.

5.4 Square summability of the thickness gradient

The Lyapunov dissipation controls the tangential gradient directly.

Theorem 5.5 (Square summability of the gradient)**.** *Every return orbit satisfies*

$$\sum_{k=0}^{\infty} |\nabla_{\partial C} d(c_k)|^2 < \infty. \tag{129}$$

More precisely,

$$\sum_{k=0}^{\infty} |\nabla_{\partial C} d(c_k)|^2 \le \frac{d_\infty - d(c_0)}{\gamma} \le \frac{d_{\max} - d(c_0)}{\gamma}. \tag{130}$$

In particular,

$$|\nabla_{\partial C} d(c_k)| \longrightarrow 0. \tag{131}$$

Proof. From the lower Lyapunov estimate,

$$\gamma |g_k|^2 \le \mathcal{D}(c_k).$$

Summing over k and using Proposition 5.4 gives

$$\gamma \sum_{k=0}^{\infty} |g_k|^2 \le \sum_{k=0}^{\infty} \mathcal{D}(c_k) = d_\infty - d(c_0),$$

which proves (130). A convergent series of nonnegative terms has terms tending to zero, so (131) follows. □

Remark 5.6. The estimate (129) is an ℓ^2-summability statement. It does not imply

$$\sum_{k=0}^{\infty} |\nabla_{\partial C} d(c_k)| < \infty.$$

Accordingly, convergence of the orbit cannot be deduced from this estimate alone.

5.5 Asymptotic regularity of the return orbit

The uniform one-step estimate now converts vanishing gradient into vanishing displacement.

Theorem 5.7 (Asymptotic regularity)**.** *Every return orbit satisfies*

$$|c_{k+1} - c_k| \longrightarrow 0. \tag{132}$$

Moreover,

$$\sum_{k=0}^{\infty} |c_{k+1} - c_k|^2 < \infty. \tag{133}$$

More precisely,

$$\sum_{k=0}^{\infty} |c_{k+1} - c_k|^2 \le \frac{C_F^2}{\gamma} \big(d_\infty - d(c_0)\big), \tag{134}$$

where C_F is the constant in (66).

Proof. By Corollary 3.6,

$$|c_{k+1} - c_k| \le C_F |\nabla_{\partial C} d(c_k)|.$$

Together with (131), this immediately gives (132).

Squaring the same inequality and summing yields

$$\sum_{k=0}^{\infty} |c_{k+1} - c_k|^2 \le C_F^2 \sum_{k=0}^{\infty} |\nabla_{\partial C} d(c_k)|^2.$$

The estimate (134) now follows from (130). □

The tangential component enjoys the same type of control. Indeed, (67) gives

$$\beta_-^2 |g_k|^2 \le \left| P_{T_{c_k}\partial C}(c_{k+1} - c_k) \right|^2 \le T_0^2 |g_k|^2. \tag{135}$$

Combining this with (111) yields the useful comparison

$$\frac{\gamma}{T_0^2} \left| P_{T_c\partial C}(F(c) - c) \right|^2 \le \mathcal{D}(c) \le \frac{\Gamma}{\beta_-^2} \left| P_{T_c\partial C}(F(c) - c) \right|^2. \tag{136}$$

Thus, in the global small-slope regime, Lyapunov dissipation, squared gradient size, and squared tangential return displacement are quantitatively comparable.

5.6 What the Lyapunov estimate does not yet prove

The preceding results establish three global facts for every return orbit:

$$d(c_k) \longrightarrow d_\infty, \tag{137}$$

$$|\nabla_{\partial C} d(c_k)| \longrightarrow 0, \tag{138}$$

and

$$|c_{k+1} - c_k| \longrightarrow 0. \tag{139}$$

These conclusions do not, by themselves, imply that the sequence (c_k) converges to a single point. In particular, square-summability of the increments does not imply absolute summability, and a sequence on a compact manifold may possess more than one accumulation point while its successive increments tend to zero.

A Kurdyka–Łojasiewicz inequality could, under additional analytic assumptions, strengthen this ℓ^2 control to a finite-length estimate and provide quantitative convergence information near nonisolated or degenerate critical sets, and also near degenerate isolated critical points. No such inequality is required for the global convergence theorem proved here.

The next section therefore addresses the remaining compactness and critical-set argument. Under an explicit isolation hypothesis on the critical points of d, we shall prove that every return orbit converges to a single critical point.

6 Global Convergence of the Return Dynamics

The Lyapunov analysis of Section 5 shows that every return orbit satisfies

$$d(c_k) \longrightarrow d_\infty,\ |\nabla_{\partial C} d(c_k)| \longrightarrow 0,\ |c_{k+1} - c_k| \longrightarrow 0.$$

These facts imply that every accumulation point is critical, but they do not by themselves force convergence to a single point.

In this section we add an isolation hypothesis on the critical set and show that it is sufficient to obtain global convergence of every return orbit.

6.1 The critical set and the isolation hypothesis

Define

$$\mathrm{Crit}(d) := \{c \in \partial C : \nabla_{\partial C} d(c) = 0\}. \tag{140}$$

Since $d \in C^2(\partial C)$ and ∂C is compact, $\mathrm{Crit}(d)$ is a compact subset of ∂C. Moreover, because d attains a maximum and a minimum on the compact manifold ∂C, the critical set is nonempty.

For the remainder of this section we impose the following hypothesis.

Critical-point isolation hypothesis. Every point of $\mathrm{Crit}(d)$ is isolated in $\mathrm{Crit}(d)$.

This assumption is strictly weaker than requiring d to be a Morse function. In particular, no nondegeneracy of the Hessian is required for the convergence theorem below.

Lemma 6.1 (Finiteness of the critical set)**.** *Under the critical-point isolation hypothesis,* $\mathrm{Crit}(d)$ *is finite.*

Proof. The set $\mathrm{Crit}(d)$ is compact. If it were infinite, compactness would imply the existence of an accumulation point $c_* \in \mathrm{Crit}(d)$. This would contradict the assumption that every critical point is isolated. Hence $\mathrm{Crit}(d)$ is finite. □

We therefore write

$$\mathrm{Crit}(d) = \left\{c^{(1)}, \dots, c^{(m)}\right\}. \tag{141}$$

By the fixed-point characterization established in [2],

$$\mathrm{Fix}(F) = \mathrm{Crit}(d). \tag{142}$$

6.2 Uniform ascent away from the critical set

The strict Lyapunov estimate gives a uniform thickness gain away from any neighborhood of the critical set.

Lemma 6.2 (Uniform ascent away from critical points)**.** *Let $U \subset \partial C$ be any open neighborhood of* $\mathrm{Crit}(d)$*. Then there exists $\varepsilon_U > 0$ such that*

$$|\nabla_{\partial C} d(c)| \geq \varepsilon_U \qquad \text{for every } c \in \partial C \setminus U. \tag{143}$$

Consequently,

$$d(F(c)) - d(c) \geq \gamma \varepsilon_U^2 \qquad \text{for every } c \in \partial C \setminus U. \tag{144}$$

Proof. The set

$$Q_U := \partial C \setminus U$$

is compact. Since U contains the entire critical set,

$$\nabla_{\partial C} d(c) \neq 0 \qquad \text{for every } c \in Q_U.$$

The continuous function

$$c \longmapsto |\nabla_{\partial C} d(c)|$$

therefore attains a strictly positive minimum on Q_U. Set

$$\varepsilon_U := \min_{c \in Q_U} |\nabla_{\partial C} d(c)| > 0.$$

This proves (143).

The strict ascent estimate (98) then gives

$$d(F(c)) - d(c) \geq \gamma |\nabla_{\partial C} d(c)|^2 \geq \gamma \varepsilon_U^2,$$

which proves (144). □

The preceding estimate gives more than asymptotic approach to the critical set: an orbit can spend only finitely many iterates outside any prescribed neighborhood of it.

Proposition 6.3 (Eventual trapping near the critical set)**.** *Let U be any open neighborhood of $\mathrm{Crit}(d)$. For every return orbit $(c_k)_{k\geq 0}$ there exists an integer K_U such that*

$$c_k \in U \qquad \text{for every } k \geq K_U. \tag{145}$$

Moreover, the number of indices for which $c_k \notin U$ satisfies

$$\#\{k \geq 0 : c_k \notin U\} \leq \frac{d_{\max} - d(c_0)}{\gamma \varepsilon_U^2}. \tag{146}$$

Proof. Whenever $c_k \notin U$, Lemma 6.2 gives

$$d(c_{k+1}) - d(c_k) \geq \gamma \varepsilon_U^2.$$

On the other hand, the total thickness gain along the orbit is bounded by

$$\sum_{k=0}^{\infty} \big(d(c_{k+1}) - d(c_k)\big) = d_\infty - d(c_0) \leq d_{\max} - d(c_0).$$

Hence the orbit can contain at most

$$\frac{d_{\max} - d(c_0)}{\gamma \varepsilon_U^2}$$

indices outside U. This proves both assertions. □

6.3 Approach to the critical set

Let

$$\mathrm{dist}\big(c, \mathrm{Crit}(d)\big) := \min_{q \in \mathrm{Crit}(d)} |c - q|.$$

Corollary 6.4 (Distance to the critical set)**.** *Every return orbit satisfies*

$$\mathrm{dist}\big(c_k, \mathrm{Crit}(d)\big) \longrightarrow 0. \tag{147}$$

Proof. For every $\rho > 0$, let

$$U_\rho := \big\{c \in \partial C : \mathrm{dist}\big(c, \mathrm{Crit}(d)\big) < \rho\big\}.$$

This is an open neighborhood of $\mathrm{Crit}(d)$. Proposition 6.3 therefore gives an integer K_ρ such that

$$c_k \in U_\rho \qquad \text{for all } k \geq K_\rho.$$

Since $\rho > 0$ is arbitrary, (147) follows. □

There is an equivalent compactness argument using

$$|\nabla_{\partial C} d(c_k)| \longrightarrow 0.$$

The formulation above is useful because it also provides the finite visit estimate (146).

6.4 Accumulation points and the omega-limit set

For an initial point $c_0 \in \partial C$, define the omega-limit set

$$\omega(c_0) := \big\{q \in \partial C : c_{k_j} \longrightarrow q \text{ for some sequence } k_j \to \infty\big\}. \tag{148}$$

Since ∂C is compact, $\omega(c_0)$ is nonempty.

Proposition 6.5 (All accumulation points are critical)**.** *For every return orbit,*

$$\omega(c_0) \subset \mathrm{Crit}(d) \cap d^{-1}(d_\infty). \tag{149}$$

In particular, every accumulation point of the orbit is a fixed point of the return map.

Proof. Let $q \in \omega(c_0)$. Then there exists a subsequence c_{k_j} such that

$$c_{k_j} \longrightarrow q.$$

By Theorem 5.5,

$$|\nabla_{\partial C} d(c_k)| \longrightarrow 0.$$

Continuity of the gradient therefore gives

$$\nabla_{\partial C} d(q) = 0.$$

Hence

$$q \in \mathrm{Crit}(d).$$

Moreover,

$$d(c_k) \longrightarrow d_\infty,$$

and continuity of d gives

$$d(q) = d_\infty.$$

Thus

$$q \in \mathrm{Crit}(d) \cap d^{-1}(d_\infty).$$

Finally, (142) gives

$$F(q) = q.$$

□

Remark 6.6. The conclusion of Proposition 6.5 does not require the critical points to be isolated. Without the isolation hypothesis, the Lyapunov theory still shows that the orbit approaches the critical set and that all its accumulation points lie on the single critical level $d = d_\infty$. What may fail without further information is convergence to one particular critical point.

6.5 Convergence to a single critical point

We now combine three ingredients:

1. eventual localization near the finite critical set;
2. vanishing one-step displacement;
3. isolation of the critical points.

The implication from gradient control, compactness, and vanishing steps to convergence in the presence of isolated critical points is a standard discrete-dynamical argument; see, for comparison, the broader framework of descent convergence in [8, 13]. The return-map contribution here is the geometric derivation of the required ascent and step-control estimates, rather than a new abstract convergence principle.

Theorem 6.7 (Global convergence). *Assume the hypotheses of Theorem 4.7 and the critical-point isolation hypothesis.*

Then, for every initial condition $c_0 \in \partial C$, there exists a unique critical point

$$c_* \in \mathrm{Crit}(d)$$

such that

$$\lim_{k\to\infty} c_k = c_*, \qquad c_{k+1} = F(c_k). \tag{150}$$

Moreover,

$$d(c_*) = d_\infty = \lim_{k\to\infty} d(c_k). \tag{151}$$

Proof. By Lemma 6.1,

$$\mathrm{Crit}(d) = \{c^{(1)}, \dots, c^{(m)}\}.$$

If $m = 1$, the conclusion follows immediately from Corollary 6.4. We therefore assume $m \geq 2$.

Choose $\rho > 0$ sufficiently small that the neighborhoods

$$U_i := \partial C \cap B_\rho(c^{(i)}), \qquad i = 1, \dots, m, \tag{152}$$

have pairwise disjoint closures and satisfy

$$\overline{U_i} \cap \mathrm{Crit}(d) = \{c^{(i)}\}. \tag{153}$$

Since there are finitely many such sets and their closures are pairwise disjoint compact subsets of ∂C,

$$\delta_{\mathrm{sep}} := \min_{i\neq j} \mathrm{dist}\big(\overline{U_i}, \overline{U_j}\big) > 0. \tag{154}$$

Set

$$U := \bigcup_{i=1}^{m} U_i.$$

By Proposition 6.3, there exists K_0 such that

$$c_k \in U \qquad \text{for every } k \geq K_0. \tag{155}$$

By Theorem 5.7,

$$|c_{k+1} - c_k| \longrightarrow 0.$$

Hence there exists $K_1 \geq K_0$ such that

$$|c_{k+1} - c_k| < \delta_{\mathrm{sep}} \qquad \text{for every } k \geq K_1. \tag{156}$$

Choose the unique index i_* such that

$$c_{K_1} \in U_{i_*}.$$

We claim that

$$c_k \in U_{i_*} \qquad \text{for every } k \geq K_1. \tag{157}$$

Indeed, suppose that for some $k \geq K_1$ one had

$$c_k \in U_i, \qquad c_{k+1} \in U_j, \qquad i \neq j.$$

Then

$$|c_{k+1} - c_k| \geq \mathrm{dist}\big(\overline{U_i}, \overline{U_j}\big) \geq \delta_{\mathrm{sep}},$$

contradicting (156). Thus the orbit cannot change critical neighborhood after time K_1, and (157) follows.

It remains to prove convergence inside U_{i_*}. Suppose, for contradiction, that

$$c_k \not\longrightarrow c^{(i_*)}.$$

Then there exist $\varepsilon > 0$ and a subsequence c_{k_j} such that

$$|c_{k_j} - c^{(i_*)}| \geq \varepsilon.$$

Since $\overline{U_{i_*}}$ is compact, after passing to a further subsequence we may assume

$$c_{k_j} \longrightarrow q \in \overline{U_{i_*}}.$$

Proposition 6.5 gives

$$q \in \mathrm{Crit}(d).$$

By (153),

$$q = c^{(i_*)},$$

contradicting

$$|q - c^{(i_*)}| \geq \varepsilon.$$

Therefore

$$c_k \longrightarrow c^{(i_*)}.$$

Setting

$$c_* := c^{(i_*)}$$

proves (150).

Finally, continuity of d and $d(c_k) \to d_\infty$ give

$$d(c_*) = d_\infty,$$

which proves (151). □

6.6 Limit map and convergence classes

The global convergence theorem defines a natural asymptotic assignment.

Definition 6.8 (Limit map)**.** For $c \in \partial C$, define

$$\mathcal{L}(c) := \lim_{k\to\infty} F^k(c). \tag{158}$$

By Theorem 6.7,

$$\mathcal{L}(c) \in \mathrm{Crit}(d)$$

for every $c \in \partial C$.

For a critical point c_*, define its convergence class by

$$\mathcal{C}(c_*) := \left\{ c \in \partial C : F^k(c) \longrightarrow c_* \right\}. \tag{159}$$

Corollary 6.9 (Partition into convergence classes)**.** *The sets*

$$\mathcal{C}(c_*), \qquad c_* \in \mathrm{Crit}(d),$$

are pairwise disjoint and satisfy

$$\partial C = \bigsqcup_{c_* \in \mathrm{Crit}(d)} \mathcal{C}(c_*). \tag{160}$$

Proof. Existence of a critical limit for every initial condition follows from Theorem 6.7. Hence the union of the convergence classes is all of ∂C.

If

$$c \in \mathcal{C}(c_*) \cap \mathcal{C}(q_*),$$

then the same sequence $F^k(c)$ converges both to c_* and to q_*. Since ∂C is Hausdorff,

$$c_* = q_*.$$

Thus the convergence classes are pairwise disjoint. □

Remark 6.10. We deliberately use the term *convergence class* rather than *basin of attraction* in (159). A critical point may be repelling or of saddle type, and its convergence class need not contain an open neighborhood of the equilibrium. The term basin of attraction will be reserved in Section 8 for attracting fixed points.

6.7 Scope of the convergence theorem

Theorem 6.7 separates the assumptions needed for global convergence into two logically distinct groups.

The geometric and dynamical assumptions of Sections 3–5 provide

$$d(c_{k+1}) - d(c_k) \geq \gamma |\nabla_{\partial C} d(c_k)|^2,$$

and therefore

$$|\nabla_{\partial C} d(c_k)| \to 0, \qquad |c_{k+1} - c_k| \to 0.$$

The critical-point isolation hypothesis is used only in the final topological step that prevents an asymptotically small-step orbit from moving indefinitely among different components of the critical set.

Accordingly, the Morse condition is not required for global convergence. It is sufficient that the critical points of the thickness function be isolated. The more refined Morse-theoretic organization of the critical set is a separate question and is not used in the present argument.

7 Local Asymptotics and Convergence Rates

The global convergence theorem determines the limit of every return orbit under the hypotheses of the preceding sections. We now refine that result near an isolated critical point by using the exact linearization established in [2].

The local behavior is governed not by the Hessian of the thickness alone, but by its interaction with the curvature-dependent preconditioner

$$B_* = d_*\big(I - d_* S_*\big)^{-1}.$$

This leads to a spectral classification in terms of the self-adjoint preconditioned Hessian

$$K_* = B_*^{1/2} H_* B_*^{1/2}.$$

7.1 Local regularity and the exact linearization

Let

$$c_* \in \mathrm{Crit}(d)$$

be an isolated critical point. Under the standing assumptions

$$\partial C \in C^3, \qquad d \in C^2(\partial C),$$

the radial map

$$\Phi(c) = c + d(c)\nu(c)$$

is of class C^2. Since the return is transverse, the first-return parameter is locally obtained from an implicit equation with a nonvanishing derivative in the return direction. Consequently, the reciprocal map and the return map

$$F = \pi \circ \Phi$$

are of class C^1 in a neighborhood of c_*.

Set

$$d_* := d(c_*), \qquad S_* := S_{c_*}, \qquad H_* := H_{c_*}, \tag{161}$$

and define

$$B_* := d_*\big(I - d_* S_*\big)^{-1}. \tag{162}$$

The exact linearization obtained in [2] is

$$DF(c_*)\big|_{T_{c_*}\partial C} = I + B_* H_*. \tag{163}$$

Introduce the self-adjoint operator

$$K_* := B_*^{1/2} H_* B_*^{1/2}. \tag{164}$$

Since

$$B_* H_* = B_*^{1/2} K_* B_*^{-1/2}, \tag{165}$$

the operators B_*H_* and K_* have the same real spectrum.

Let

$$\mu_1, \dots, \mu_{N-1} \tag{166}$$

denote the eigenvalues of K_*. Then the multipliers of the return map are

$$\lambda_j = 1 + \mu_j, \qquad j = 1, \dots, N-1. \tag{167}$$

Moreover, by Sylvester's law of inertia, K_* and H_* have the same numbers of positive, negative, and zero eigenvalues.

7.2 Local asymptotic form of the iteration

Choose a C^2 local coordinate chart

$$\chi : U \subset \partial C \longrightarrow T_{c_*}\partial C$$

such that

$$\chi(c_*) = 0, \qquad D\chi(c_*) = I.$$

Define the local representation

$$\widehat{F} := \chi \circ F \circ \chi^{-1}. \tag{168}$$

Then

$$\widehat{F}(0) = 0$$

and, by (163),

$$D\widehat{F}(0) = A_*, \qquad A_* := I + B_* H_*. \tag{169}$$

Hence

$$\widehat{F}(u) = A_* u + \psi_*(u), \tag{170}$$

where

$$\frac{|\psi_*(u)|}{|u|} \longrightarrow 0 \qquad \text{as } u \to 0. \tag{171}$$

Thus, if

$$u_k := \chi(c_k)$$

for an orbit converging to c_*, then

$$u_{k+1} = A_* u_k + o(|u_k|). \tag{172}$$

Equation (172) is the local asymptotic model of the nonlinear return dynamics.

7.3 Spectral classification of critical points

The exact multipliers

$$\lambda_j = 1 + \mu_j$$

give the following classification.

Proposition 7.1 (Local spectral alternatives)**.** *Let c_* be a nondegenerate critical point of d.*

1. *If c_* is a strict local minimum, then*

$$\mu_j > 0 \qquad \textit{for every } j,$$

and hence

$$\lambda_j > 1 \qquad \textit{for every } j. \tag{173}$$

Thus c_* is a hyperbolic repelling fixed point.

2. *If c_* is a strict local maximum, then*

$$\mu_j < 0 \qquad \textit{for every } j.$$

It is linearly attracting if and only if

$$-2 < \mu_j < 0 \qquad \textit{for every } j. \tag{174}$$

Equivalently,

$$|\lambda_j| < 1 \qquad \textit{for every } j. \tag{175}$$

3. *If c_* is a nondegenerate saddle point, then K_* has both positive and negative eigenvalues. In particular, at least one multiplier satisfies*

$$\lambda_j > 1, \tag{176}$$

so c_* is unstable.

The condition

$$\mu_j < 0$$

at a local maximum is therefore not sufficient for attraction. The quantitative lower bound

$$\mu_j > -2$$

is also necessary.

If some

$$\mu_j = -2,$$

then the corresponding multiplier is

$$\lambda_j = -1,$$

and the fixed point is nonhyperbolic in that direction. If

$$\mu_j < -2,$$

then

$$\lambda_j < -1,$$

and the maximum is unstable in that direction.

7.4 Compatibility with the global ascent condition

The spectral sufficient condition introduced in Section 4.3 was

$$\lambda_{\min}(K_c) \geq -2 + \delta \qquad \text{for every } c \in \partial C, \tag{177}$$

for some $\delta > 0$.

At a nondegenerate local maximum c_*, all eigenvalues of K_* are negative. Hence (177) implies

$$-2 + \delta \leq \mu_j < 0, \qquad j = 1, \dots, N-1. \tag{178}$$

Consequently,

$$-1 + \delta \leq \lambda_j < 1. \tag{179}$$

Thus every nondegenerate local maximum is attracting under the uniform spectral ascent condition.

Similarly, at a nondegenerate saddle point the positive eigenvalues of K_* produce multipliers larger than one, while the negative eigenvalues lie in $(-2, 0)$. Hence, under (177), every nondegenerate saddle has both stable and unstable spectral directions.

This exhibits the same threshold -2 at the global and local levels: globally it guarantees positivity of the quadratic ascent form, while locally it prevents the multipliers associated with negative curvature of the thickness landscape from crossing the value -1.

7.5 Exponential convergence to an attracting maximum

We now quantify the convergence of an orbit whose limiting critical point is hyperbolically attracting. Exponential convergence from a C^1 fixed-point linearization with spectral radius less than one is classical (see, e.g., [14, 15]). The specialization below identifies its rate explicitly through the geometry-induced operator K_*.

Define

$$\rho_* := \rho\big(DF(c_*)\big) = \max_{1 \leq j \leq N-1} |1 + \mu_j|, \tag{180}$$

where $\rho(\cdot)$ denotes the spectral radius.

Theorem 7.2 (Local exponential convergence)**.** *Let c_* be a nondegenerate critical point satisfying*

$$\rho_* < 1. \tag{181}$$

Then c_* is a strict local maximum of d.

For every number

$$\rho_* < q < 1, \tag{182}$$

there exist a neighborhood U_* of c_* and a constant $C_q > 0$ such that every orbit entering U_* and remaining there satisfies

$$|c_k - c_*| \leq C_q q^{k-k_0} |c_{k_0} - c_*| \tag{183}$$

for all $k \geq k_0$.

In particular, if a global orbit satisfies

$$c_k \longrightarrow c_*,$$

then (183) holds for all sufficiently large k.

Proof. Since

$$\rho(A_*) = \rho_* < 1,$$

finite-dimensional linear algebra provides a norm $\|\cdot\|_*$ on $T_{c_*}\partial C$, equivalent to the Euclidean norm, such that

$$\|A_*\|_* < q. \tag{184}$$

After replacing q by an intermediate number if necessary, choose q_0 such that

$$\|A_*\|_* < q_0 < q < 1.$$

Since $\widehat{F}$ is C^1 and

$$D\widehat{F}(0) = A_*,$$

there exists $r_* > 0$ such that

$$\|D\widehat{F}(u)\|_* \leq q \qquad \text{whenever } \|u\|_* < r_*. \tag{185}$$

The mean-value estimate therefore gives

$$\|\widehat{F}(u)\|_* \leq q\|u\|_* \tag{186}$$

for $\|u\|_* < r_*$.

Iterating,

$$\|u_k\|_* \le q^{k-k_0}\|u_{k_0}\|_*. \tag{187}$$

Equivalence of the local coordinate norm, the Euclidean norm, and $\|\cdot\|_*$ gives (183).

It remains to identify the critical type. Since

$$|1+\mu_j| < 1,$$

one has

$$-2 < \mu_j < 0$$

for every j. Thus K_* is negative definite. By Sylvester's law of inertia, H_* is negative definite as well, and c_* is a strict local maximum of d. □

Remark 7.3. The theorem yields an exponential estimate with every rate $q > \rho_*$. It does not assert that every orbit converging to c_* has the exact asymptotic rate ρ_*. An orbit may lie in a faster spectral direction, so its observed decay can be strictly faster than the spectral radius.

7.6 Rates for thickness, gradient, and return displacement

The exponential convergence of the configuration gives corresponding rates for the geometric quantities governing the dynamics.

Proposition 7.4 (Derived local convergence rates)**.** *Let the assumptions of Theorem 7.2 hold, and suppose*

$$c_k \longrightarrow c_*.$$

For every q satisfying

$$\rho_* < q < 1,$$

there exist constants

$$C_d > 0, \qquad C_g > 0, \qquad C_s > 0,$$

and an index K such that, for every $k \ge K$,

$$0 \le d(c_*) - d(c_k) \le C_d q^{2k}, \tag{188}$$

$$|\nabla_{\partial C} d(c_k)| \le C_g q^k, \tag{189}$$

$$|c_{k+1} - c_k| \le C_s q^k. \tag{190}$$

Proof. Because c_* is a nondegenerate local maximum, H_* is negative definite. In local coordinates centered at c_*, Taylor's theorem gives

$$d(c_*) - d(c) = -\frac{1}{2}\langle H_* u, u\rangle + o(|u|^2), \tag{191}$$

where

$$u = \chi(c).$$

Hence there exists $C > 0$ such that

$$0 \le d(c_*) - d(c) \le C|c - c_*|^2 \tag{192}$$

for c sufficiently close to c_*.

Using Theorem 7.2 gives

$$d(c_*) - d(c_k) \le C_d q^{2k}$$

after absorbing the finite entry time into the constant.

Since

$$\nabla_{\partial C} d(c_*) = 0$$

and the gradient is C^1,

$$|\nabla_{\partial C} d(c)| \le C|c - c_*| \tag{193}$$

near c_*. The exponential position estimate therefore yields (189).

Finally, the global one-step estimate (66) gives

$$|c_{k+1} - c_k| \le C_F |\nabla_{\partial C} d(c_k)|,$$

and (190) follows. □

Thus, near a nondegenerate attracting maximum, the configuration, gradient, and step size decay geometrically at first order, whereas the remaining thickness deficit decays at twice the exponent:

$$|c_k - c_*|,\ |\nabla d(c_k)|,\ |c_{k+1} - c_k| = O(q^k),$$

while

$$d(c_*) - d(c_k) = O(q^{2k}).$$

7.7 Possible limits of globally convergent orbits

Theorem 6.7 states that every orbit converges to a critical point under the global hypotheses. The local classification explains how such convergence can occur.

If the limiting point is an attracting nondegenerate maximum, then the convergence is robust under perturbation of the initial condition and is exponentially fast by Theorem 7.2.

If the limiting point is a nondegenerate minimum, then all local multipliers satisfy

$$\lambda_j > 1.$$

Thus the equilibrium is locally repelling. Convergence to such a point cannot occur through ordinary local

attraction; an orbit converging to it must belong to an exceptional convergence class, for example by reaching the fixed point exactly after finitely many iterations.

At a saddle point, at least one multiplier satisfies

$$\lambda_j > 1.$$

Hence convergence can occur only through dynamically restricted initial data associated with stable directions. A precise description of these convergence classes requires additional local invariant-manifold hypotheses and will be separated from the global convergence statement.

Thus global convergence to *some critical point* does not mean that every critical point is an attractor. The global Lyapunov structure and the local stability type answer different questions.

8 Convergence Classes, Attraction Basins, and Absence of Recurrence

The global convergence theorem gives a partition of the phase space according to the limiting critical point of each orbit. The distinction between attraction basins and exceptional convergence to unstable fixed points is familiar from hyperbolic dynamics [14] and from the analysis of gradient descent, whose iterates avoid saddle points except for a set of exceptional initial data [16]. This partition should be distinguished from the decomposition into basins of attraction: a critical point may be a global limit for exceptional initial data without being locally attracting.

In this section we make this distinction precise. We also show that the strict Lyapunov structure excludes all nontrivial periodic and recurrent dynamics in the global ascent regime.

8.1 Convergence classes and attraction basins

Recall from Section 6.6 that, for every $c_* \in \mathrm{Crit}(d)$, its convergence class is

$$\mathcal{C}(c_*) := \left\{ c \in \partial C : F^k(c) \longrightarrow c_* \right\}. \tag{194}$$

Under the hypotheses of Theorem 6.7,

$$\partial C = \bigsqcup_{c_* \in \mathrm{Crit}(d)} \mathcal{C}(c_*). \tag{195}$$

We reserve the term *basin of attraction* for critical points that are locally attracting.

Definition 8.1 (Basin of attraction)**.** Let c_* be an attracting fixed point of F. Its basin of attraction is

$$\mathcal{B}(c_*) := \left\{ c \in \partial C : F^k(c) \longrightarrow c_* \right\}. \tag{196}$$

Thus, as a set,

$$\mathcal{B}(c_*) = \mathcal{C}(c_*),$$

but the notation $\mathcal{B}(c_*)$ is used only when c_* is attracting.

This terminology separates a dynamical property of the equilibrium from the mere existence of convergent initial conditions.

8.2 Global ascent and the local spectrum

The strict ascent inequality places an additional restriction on the local spectrum of every nondegenerate critical point.

Proposition 8.2 (Spectral consequence of strict global ascent)**.** *Assume that*

$$d(F(c)) - d(c) \geq \gamma |\nabla_{\partial C} d(c)|^2 \tag{197}$$

holds in a neighborhood of a nondegenerate critical point c_*, with $\gamma > 0$.

Let

$$\mu$$

be an eigenvalue of

$$K_* = B_*^{1/2} H_* B_*^{1/2}.$$

Then

$$\mu < 0 \quad \Longrightarrow \quad -2 < \mu < 0. \tag{198}$$

Consequently, the corresponding multiplier

$$\lambda = 1 + \mu$$

satisfies

$$|\lambda| < 1. \tag{199}$$

Proof. Let $y \neq 0$ be an eigenvector of the self-adjoint operator K_* associated with μ, and set

$$v := B_*^{1/2} y \in T_{c_*} \partial C.$$

Since

$$B_* H_* = B_*^{1/2} K_* B_*^{-1/2},$$

we have $B_* H_* v = \mu v$. Thus, with $A_* := DF(c_*) = I + B_* H_*$,

$$A_* v = (1 + \mu) v. \tag{200}$$

Choose the smooth curve

$$c(s) := \exp_{c_*}(sv)$$

on ∂C for $|s|$ small. In ambient coordinates, $c(s) = c_* + sv + O(s^2)$. Since c_* is critical,

$$d(c(s)) = d(c_*) + \frac{s^2}{2}\langle H_* v, v\rangle + o(s^2). \tag{201}$$

The local linearization gives

$$F(c(s)) = c_* + s(1+\mu)v + o(s),$$

and hence

$$d(F(c(s))) = d(c_*) + \frac{s^2}{2}(1+\mu)^2\langle H_* v, v\rangle + o(s^2). \tag{202}$$

Subtracting,

$$d(F(c(s))) - d(c(s)) = \frac{s^2}{2}\left((1+\mu)^2 - 1\right)\langle H_* v, v\rangle + o(s^2). \tag{203}$$

Since

$$B_* H_* v = \mu v,$$

one has

$$H_* v = \mu B_*^{-1} v,$$

and therefore

$$\langle H_* v, v\rangle = \mu \langle B_*^{-1} v, v\rangle. \tag{204}$$

Because B_*^{-1} is positive definite, the sign of $\langle H_* v, v\rangle$ is the sign of μ.

Suppose now that $\mu < 0$. Then

$$\langle H_* v, v\rangle < 0.$$

On the other hand,

$$\nabla_{\partial C} d(c(s)) = sH_* v + o(s),$$

so the right-hand side of (197) is strictly positive to order s^2. Therefore the coefficient of s^2 in (203) must be positive. Since $\langle H_* v, v\rangle < 0$, this forces

$$(1+\mu)^2 - 1 < 0.$$

Equivalently,

$$|1+\mu| < 1,$$

which is precisely

$$-2 < \mu < 0.$$

□

Corollary 8.3 (Nondegenerate critical points in the ascent regime)**.** *Under the strict global ascent hypotheses:*

1. *every nondegenerate local maximum is a hyperbolic attracting fixed point;*
2. *every nondegenerate local minimum is a hyperbolic repelling fixed point;*
3. *every nondegenerate saddle has both stable and unstable spectral directions.*

Proof. At a nondegenerate maximum, every eigenvalue μ_j of K_* is negative. Proposition 8.2 gives

$$-2 < \mu_j < 0$$

for every j, so

$$|1+\mu_j| < 1.$$

At a nondegenerate minimum, every $\mu_j > 0$, hence

$$1 + \mu_j > 1.$$

At a nondegenerate saddle, K_* has both positive and negative eigenvalues. The positive ones yield multipliers larger than one, whereas Proposition 8.2 places the negative ones inside the unit disk. □

This result shows that, inside the global monotone regime, the local and global theories are fully compatible: nondegenerate maxima are the local attractors of the thickness-ascent dynamics.

8.3 Openness of attraction basins

Proposition 8.4 (Openness of an attraction basin)**.** *Let c_* be an attracting fixed point of F. Then its basin $\mathcal{B}(c_*)$ is open in ∂C.*

Proof. Since c_* is attracting, there exists an open neighborhood U_* of c_* such that

$$F(U_*) \subset U_* \tag{205}$$

and every orbit starting in U_* converges to c_*.

Let

$$c \in \mathcal{B}(c_*).$$

Then

$$F^k(c) \longrightarrow c_*,$$

so there exists an integer $m \geq 0$ such that

$$F^m(c) \in U_*.$$

Since F^m is continuous, there exists an open neighborhood W of c satisfying

$$F^m(W) \subset U_*.$$

Every point of W therefore converges to c_*, and hence

$$W \subset \mathcal{B}(c_*).$$

Thus $\mathcal{B}(c_*)$ is open. □

Let

$$\mathcal{A} := \{c_* \in \mathrm{Crit}(d) : c_* \text{ is attracting}\}. \tag{206}$$

Then

$$\mathfrak{B} := \bigcup_{c_* \in \mathcal{A}} \mathcal{B}(c_*) \tag{207}$$

is an open subset of ∂C.

8.4 Repelling critical points

The convergence class of a repelling fixed point has a very different structure. The local inverse contraction argument used below is a standard consequence of hyperbolic fixed-point theory (see [14, 15]); its application here concerns the preimages of a critical point of the geometrically defined map F.

Proposition 8.5 (Convergence to a hyperbolic repeller)**.** *Let c_* be a hyperbolic repelling fixed point, so that every multiplier of $DF(c_*)$ has modulus strictly larger than one. Then*

$$\mathcal{C}(c_*) = \bigcup_{m=0}^{\infty} F^{-m}(\{c_*\}). \tag{208}$$

In other words, an orbit converges to c_* if and only if it reaches c_* exactly after finitely many iterations.

Proof. The inclusion from right to left is immediate because c_* is a fixed point.

For the converse, let

$$F^k(c) \longrightarrow c_*.$$

Since every multiplier of $DF(c_*)$ has modulus larger than one, $DF(c_*)$ is invertible and

$$\rho\big(DF(c_*)^{-1}\big) < 1.$$

The inverse-function theorem therefore gives neighborhoods U and V of c_* such that

$$F : U \longrightarrow V$$

is a diffeomorphism onto its image, with inverse $G : V \to U$ and $G(c_*) = c_*$. Since $DG(c_*) = DF(c_*)^{-1}$ has spectral radius strictly smaller than one, choose an adapted norm and a smaller neighborhood $W \subset U \cap V$ of c_* such that $G(W) \subset W$ and there exists $q \in (0,1)$ with

$$\|G(x) - c_*\|_* \le q\|x - c_*\|_* \tag{209}$$

for every $x \in W$.

Since $F^k(c) \to c_*$, there exists k_0 such that

$$c_k := F^k(c) \in W \qquad \text{for every } k \ge k_0.$$

For each $k \ge k_0$, both c_k and c_{k+1} lie in $W \subset U \cap V$, so the local inverse identity gives $c_k = G(c_{k+1})$. Iterating this identity yields, for every $n \ge 1$,

$$c_{k_0} = G^n(c_{k_0+n}),$$

and therefore

$$\|c_{k_0} - c_*\|_* \le q^n \|c_{k_0+n} - c_*\|_*.$$

Letting $n \to \infty$ gives

$$c_{k_0} = c_*.$$

Hence the original orbit reaches c_* after finitely many steps. □

In particular, if c_* is a nondegenerate local minimum, then Corollary 8.3 shows that (208) applies.

Thus convergence to a repelling minimum is possible only through finite preimages of the fixed point; it is not an attraction phenomenon.

8.5 Saddle convergence classes

Let c_* be a nondegenerate saddle point. Under the global ascent hypotheses, the spectrum splits into

$$|\lambda_j| < 1$$

for the directions corresponding to negative eigenvalues of K_*, and

$$\lambda_j > 1$$

for those corresponding to positive eigenvalues.

The convergence class

$$\mathcal{C}(c_*)$$

therefore consists of dynamically restricted initial conditions; it does not contain a neighborhood of c_*.

We do not identify $\mathcal{C}(c_*)$ globally with a stable manifold under the standing assumptions alone. Such an identification requires additional hypotheses concerning local invertibility, hyperbolicity, and the global intersection structure of invariant manifolds.

Remark 8.6. If, in addition,

$$0 \notin \sigma(DF(c_*)),$$

then F is a local diffeomorphism near c_*. The classical stable manifold theorem [14] may then be applied to the hyperbolic fixed point. Locally, the set of points whose forward iterates remain near c_* and converge to it is a smooth stable manifold whose dimension equals the number of multipliers satisfying

$$|\lambda_j| < 1.$$

This additional structure is not needed for the global convergence results of the present paper.

8.6 Absence of nontrivial periodic orbits

The strict Lyapunov function rules out periodic recurrence without any additional local stability assumption.

Theorem 8.7 (No nontrivial periodic orbits)**.** *Assume the strict ascent estimate* (98)*. Then F admits no periodic orbit of period $p \geq 2$. Every periodic point is a fixed point.*

Proof. Suppose that

$$c_0, c_1, \dots, c_{p-1}$$

is a periodic orbit, with

$$c_{j+1} = F(c_j), \qquad c_p = c_0.$$

Summing the strict thickness inequality over one period gives

$$\begin{aligned} 0 &= d(c_p) - d(c_0) \\ &= \sum_{j=0}^{p-1} \big(d(c_{j+1}) - d(c_j)\big) \\ &\geq \gamma \sum_{j=0}^{p-1} |\nabla_{\partial C} d(c_j)|^2. \end{aligned} \tag{210}$$

Every term on the right-hand side is nonnegative. Hence

$$\nabla_{\partial C} d(c_j) = 0$$

for every j.

By the fixed-point characterization,

$$F(c_j) = c_j.$$

Since also

$$F(c_j) = c_{j+1},$$

we obtain

$$c_{j+1} = c_j$$

for every j. Thus the orbit is constant and has period one. □

Remark 8.8. Theorem 8.7 does not require the critical points to be isolated and does not use the global convergence theorem. Strict monotonicity of the thickness alone excludes every nonconstant periodic orbit.

8.7 Absence of nontrivial recurrent points

We now use the global convergence theorem to exclude a broader form of recurrence.

Definition 8.9 (Positive recurrence)**.** A point $c \in \partial C$ is called recurrent if there exists a sequence of integers

$$k_j \longrightarrow \infty$$

such that

$$F^{k_j}(c) \longrightarrow c. \tag{211}$$

Theorem 8.10 (Recurrent points are fixed points)**.** *Under the hypotheses of Theorem 6.7,*

$$\mathrm{Rec}(F) = \mathrm{Fix}(F) = \mathrm{Crit}(d), \tag{212}$$

where $\mathrm{Rec}(F)$ denotes the set of recurrent points.

Proof. Every fixed point is trivially recurrent.

Conversely, let c be recurrent. By Theorem 6.7, there exists a critical point c_* such that

$$F^k(c) \longrightarrow c_*.$$

Therefore every subsequence of the orbit converges to the same point c_*. In particular, if

$$F^{k_j}(c) \longrightarrow c,$$

then uniqueness of limits gives

$$c = c_*.$$

Hence c is critical and therefore fixed. □

An immediate consequence is that

$$\omega(c) = \{\mathcal{L}(c)\} \tag{213}$$

for every $c \in \partial C$. Thus no orbit possesses a nontrivial omega-limit cycle or more complicated positive-time recurrent set within the global ascent regime.

8.8 Phase-space organization

The preceding results give a precise global decomposition without requiring a Morse–Smale description.

Let

$$\mathcal{A} \subset \mathrm{Crit}(d)$$

denote the attracting critical points and define the set of nonattracting critical points by

$$\mathcal{N} := \mathrm{Crit}(d) \setminus \mathcal{A}. \tag{214}$$

Then the convergence-class partition may be written as

$$\partial C = \left(\bigsqcup_{a \in \mathcal{A}} \mathcal{B}(a) \right) \bigsqcup \left(\bigsqcup_{q \in \mathcal{N}} \mathcal{C}(q) \right). \tag{215}$$

The first union is open. The second contains the exceptional convergence classes associated with repelling, saddle-type, or possibly degenerate critical points.

Throughout the remainder of this subsection, interiors and boundaries are taken relative to the phase space ∂C.

Proposition 8.11 (Location of attraction-basin boundaries)**.** *Let $a \in \mathcal{A}$. Then*

$$\partial \mathcal{B}(a) \subset \partial C \setminus \bigcup_{b \in \mathcal{A}} \mathcal{B}(b). \tag{216}$$

Consequently,

$$\partial \mathcal{B}(a) \subset \bigsqcup_{q \in \mathcal{N}} \mathcal{C}(q). \tag{217}$$

Proof. Every attraction basin $\mathcal{B}(b)$ is open by Proposition 8.4, and distinct convergence classes are disjoint.

Suppose that

$$x \in \mathcal{B}(b)$$

for some attracting critical point b. Since $\mathcal{B}(b)$ is open, there exists a neighborhood U of x contained in $\mathcal{B}(b)$.

If $b \neq a$, then

$$U \cap \mathcal{B}(a) = \varnothing,$$

so x cannot belong to the boundary of $\mathcal{B}(a)$. If $b = a$, then x lies in the interior of $\mathcal{B}(a)$ and again cannot belong to its boundary.

Thus no point of an attracting basin belongs to $\partial \mathcal{B}(a)$, proving (216). The partition (215) then yields (217). □

Remark 8.12 (No generic separatrix claim). Proposition 8.11 is intentionally weaker than a statement identifying basin boundaries with stable manifolds of saddle points. Such an identification generally requires additional hypotheses, for example hyperbolicity of all relevant equilibria, local or global invertibility, and suitable transversality assumptions of Morse–Smale type; see, for example, [15].

None of these assumptions is needed for the convergence theorem, and we therefore do not impose them here.

8.9 Global gradient-like structure

The results obtained so far may be summarized as follows.

Theorem 8.13 (Global Lyapunov structure)**.** *Assume the hypotheses of Theorem 6.7. Then the return map*

$$F : \partial C \longrightarrow \partial C$$

has the following properties:

1. $$\mathrm{Fix}(F) = \mathrm{Crit}(d),$$

   and this set is finite;

2. $$\mathcal{V}(c) = d_{\max} - d(c)$$

   is a strict Lyapunov function:

   $$\mathcal{V}(F(c)) < \mathcal{V}(c)$$

   for every nonfixed point;

3. *every orbit converges to a unique critical point;*
4. *the phase space is partitioned into convergence classes;*
5. *the convergence class of every attracting critical point is an open basin of attraction;*
6. *there are no periodic orbits of period greater than one;*
7. *the recurrent set is exactly the fixed-point set.*

Thus, under the global ascent assumptions, the return dynamics has a gradient-like structure in the Lyapunov sense [17]: thickness increases strictly along every nonstationary orbit, all positive-time orbits converge to equilibria, and nontrivial recurrent behavior is excluded.

9 Exact Unit-Circle Dynamics and the Breakdown of Monotonicity

The preceding sections establish global convergence under explicit geometric and spectral hypotheses. We now examine these conditions in the planar unit-circle geometry, where the return map is available in exact form.

This setting serves two purposes. First, it provides a direct numerical test of the thickness-ascent mechanism derived above. Second, because the map can be evaluated without replacing the geometric return by a first-order approximation, it allows us to investigate what happens when the sufficient global ascent conditions cease to hold.

9.1 Exact return map on the unit circle

Let

$$C = B_1(0) \subset \mathbb{R}^2, \qquad c(\theta) = (\cos\theta, \sin\theta),$$

and let

$$e_\theta = (-\sin\theta, \cos\theta)$$

denote the positively oriented unit tangent.

For the unit circle,

$$\nu(\theta) = c(\theta), \qquad S = -I,$$

and hence

$$B(\theta) = \frac{d(\theta)}{1 + d(\theta)}. \tag{218}$$

Following [2], define

$$p(\theta) := \frac{d'(\theta)}{1 + d(\theta)}. \tag{219}$$

The exact inward normal to the outer boundary is

$$n(\Phi(c(\theta))) = \frac{-c(\theta) + p(\theta)e_\theta}{\sqrt{1 + p(\theta)^2}}. \tag{220}$$

Introduce the radicand

$$\mathscr{R}(\theta) := 1 - d(\theta)\big(2 + d(\theta)\big)p(\theta)^2. \tag{221}$$

Whenever

$$\mathscr{R}(\theta) \geq 0,$$

the first-intersection branch is

$$\sigma(\theta) = \frac{1 + d(\theta) - \sqrt{\mathscr{R}(\theta)}}{1 + p(\theta)^2}. \tag{222}$$

Set

$$a(\theta) = 1 + d(\theta) - \sigma(\theta), \qquad b(\theta) = \sigma(\theta)p(\theta). \tag{223}$$

Then

$$a(\theta)^2 + b(\theta)^2 = 1, \tag{224}$$

and the exact return point is

$$F(c(\theta)) = a(\theta)c(\theta) + b(\theta)e_\theta. \tag{225}$$

Thus the exact angular displacement is

$$\delta(\theta) = \operatorname{atan2}\big(b(\theta), a(\theta)\big), \tag{226}$$

and the induced circle map is

$$T(\theta) = \theta + \delta(\theta) \pmod{2\pi}. \tag{227}$$

All numerical experiments below are performed with (219)–(227). No first-order return formula is used to generate the iterates.

9.2 One-dimensional specialization of the spectral condition

Since the tangent space of the unit circle is one-dimensional, the preconditioned Hessian becomes the scalar

$$K(\theta) = \frac{d(\theta)}{1 + d(\theta)}d''(\theta). \tag{228}$$

Consequently, the spectral sufficient condition of Proposition 4.5 reduces to

$$K(\theta) \geq -2 + \delta \qquad \text{for every } \theta \tag{229}$$

for some $\delta > 0$.

We consider the family

$$d(\theta) = d_0 + \varepsilon\cos(m\theta), \qquad d_0 > \varepsilon > 0, \qquad m \in \mathbb{N}. \tag{230}$$

Then

$$d'(\theta) = -m\varepsilon\sin(m\theta), \tag{231}$$

$$d''(\theta) = -m^2\varepsilon\cos(m\theta), \tag{232}$$

and therefore

$$p(\theta) = -\frac{m\varepsilon\sin(m\theta)}{1 + d_0 + \varepsilon\cos(m\theta)}. \tag{233}$$

The preconditioned Hessian is

$$K(\theta) = -m^2\varepsilon\cos(m\theta)\frac{d_0 + \varepsilon\cos(m\theta)}{1 + d_0 + \varepsilon\cos(m\theta)}. \tag{234}$$

Its minimum occurs at the local maxima of the thickness, where $\cos(m\theta) = 1$, and is

$$K_{\min} = -m^2\varepsilon\frac{d_0+\varepsilon}{1+d_0+\varepsilon}. \tag{235}$$

At such a maximum θ_*, the exact local multiplier is

$$T'(\theta_*) = 1 - m^2\varepsilon\frac{d_0+\varepsilon}{1+d_0+\varepsilon}. \tag{236}$$

Thus the local threshold

$$m^2\varepsilon\frac{d_0+\varepsilon}{1+d_0+\varepsilon} = 2 \tag{237}$$

corresponds exactly to

$$K_{\min} = -2$$

and

$$T'(\theta_*) = -1.$$

This gives an explicit one-dimensional realization of the same threshold that appeared in the general global and local theories. The scalar inequality is the specialization of Proposition 4.5, not a new independent one-dimensional convergence theorem. In particular, global strict ascent still requires the small-slope and other hypotheses of Theorem 4.7. The multiplier threshold -1 and its association with flip-type behavior are standard in one-dimensional discrete dynamics [14, 18]; the distinctive feature here is their occurrence in the exact geometric return map.

9.3 Exact-map numerical comparison of three regimes

We compare three cosine profiles. The first two remain on the $K > -2$ side of the spectral threshold, whereas the third crosses it.

The computations in this section use the exact return formula, but they do not attempt to verify the quantitative constant ε_{asc} in Theorem 4.7. Accordingly, the first two profiles are not asserted to satisfy every sufficient hypothesis of that theorem. They are exact-map numerical diagnostics organized by the spectral quantity K.

For the three profiles considered below, global reality of the first-intersection branch can nevertheless be checked algebraically, rather than inferred from a finite grid. Write

$$x = \cos(m\theta), \qquad D(x) = 1 + d_0 + \varepsilon x.$$

Then

$$\begin{aligned}\mathscr{R}(\theta) &= \frac{N(x)}{D(x)^2},\\ N(x) &= D(x)^2 - m^2\varepsilon^2(1-x^2)\big(D(x)^2-1\big).\end{aligned} \tag{238}$$

Since $d > 0$, one has $D(x) > 1$ on $[-1,1]$. For the three parameter choices in Table 1, the corresponding quartic numerators are

$$N_1(x) = \frac{16x^4 + 240x^3 + 584x^2 + 1260x + 5125}{2500}, \tag{239}$$

$$N_2(x) = \frac{4\big(36x^4 + 288x^3 + 340x^2 - 88x + 49\big)}{625}, \tag{240}$$

$$\begin{aligned}N_3(x) = \frac{236196x^4 + 3018060x^3 + 7784829x^2}{1562500}\\ + \frac{-430560x + 447100}{1562500}.\end{aligned} \tag{241}$$

For each of the three polynomials, the Sturm variation count satisfies

$$V_{N_i}(-1) = V_{N_i}(1) = 1, \qquad i = 1,2,3,$$

so the number of zeros of N_i in $(-1,1)$ is zero. Since $N_i(-1) > 0$, each polynomial is strictly positive throughout $[-1,1]$. Hence

$$\mathscr{R}(\theta) > 0 \qquad \text{for all } \theta \in [0,2\pi] \tag{242}$$

for all three profiles. Thus the exact first-intersection branch is globally real in each example. The decimal values of $\min \mathscr{R}$ reported below are numerical diagnostics and are not used to establish this positivity.

By (242), the exact first-intersection branch (222) is globally real in all three examples. The third profile can therefore be studied beyond the -2 threshold without conflating loss of monotonicity with loss of reality of the return formula.

9.4 Numerically observed monotonicity in a subcritical regime

Consider first

$$d(\theta) = 0.5 + 0.2\cos(2\theta). \tag{243}$$

For this profile,

$$K_{\min} = -0.329411\ldots, \tag{244}$$

well above the threshold -2.

The local maxima occur at

$$\theta = 0, \pi,$$

Table 1. Exact-map diagnostics for three thickness profiles. The displayed values of $\min \mathscr{R}$ and $\max |p|$ are numerical evaluations over $\theta \in [0, 2\pi]$; global positivity of $\mathscr{R}$ is established algebraically in (242). The last two columns follow from the explicit one-dimensional formulas for K and the fixed-point multiplier.

$d(\theta)$	$\min \mathscr{R}$	$\max \lvert p \rvert$	$\min K$	$T'(\theta_{\max})$
$0.5 + 0.2\cos(2\theta)$	0.910160	0.269069	-0.329412	0.670588
$0.6 + 0.4\cos(3\theta)$	0.103019	0.774597	-1.800000	-0.800000
$1.3 + 0.36\cos(3\theta)$	0.052857	0.475425	-2.021955	-1.021955

and their exact multiplier is

$$T'(\theta_{\max}) = 0.670588\ldots. \tag{245}$$

The local minima occur at

$$\theta = \frac{\pi}{2}, \frac{3\pi}{2},$$

and are repelling.

A uniform numerical evaluation of the exact map (227) on 5×10^5 equally spaced points gave

$$d(T(\theta)) - d(\theta) \geq 0 \tag{246}$$

at every sampled point. Equality occurred only at the critical points up to floating-point tolerance. No negative thickness increment was detected.

For sampled points satisfying

$$|d'(\theta)| > 10^{-5},$$

the numerical ratio

$$\frac{d(T(\theta)) - d(\theta)}{|d'(\theta)|^2} \tag{247}$$

remained between approximately

$$0.2521 \quad \text{and} \quad 0.3485. \tag{248}$$

Thus, on this numerical grid, the exact map exhibits the quadratic thickness-gain behavior predicted by the Lyapunov estimate of Section 5. This observation is not used as a verification of the quantitative small-slope hypothesis of Theorem 4.7.

9.5 Alternating convergence below the threshold

The second profile is

$$d(\theta) = 0.6 + 0.4\cos(3\theta). \tag{249}$$

This example was already used in [2] to validate the local multiplier at $\theta_* = 0$.

Here

$$d(0) = 1, \qquad d''(0) = -3.6, \tag{250}$$

so

$$K(0) = \frac{1}{2}(-3.6) = -1.8, \tag{251}$$

and therefore

$$T'(0) = -0.8. \tag{252}$$

Thus the maximum is attracting, but the negative multiplier produces an alternating approach to the equilibrium. The value -1.8 is close to, but still strictly above, the threshold -2.

A phase-wide evaluation of the exact map again detected no negative value of

$$d(T(\theta)) - d(\theta).$$

This numerical experiment therefore illustrates that oscillation of the signed coordinate around a maximum is compatible with an observed monotone increase of the thickness along the sampled exact-map data.

9.6 Crossing the -2 threshold

We now consider

$$d(\theta) = 1.3 + 0.36\cos(3\theta). \tag{253}$$

The thickness remains strictly positive:

$$0.94 \leq d(\theta) \leq 1.66.$$

The exact positivity statement (242) applies to this profile. A numerical minimization gives

$$\min_{\theta} \mathscr{R}(\theta) \approx 0.0528565, \tag{254}$$

consistent with the algebraic certification above.

At each local maximum,

$$\begin{aligned} K_{\min} &= -9(0.36)\frac{1.66}{2.66} \\ &\approx -2.0219549. \end{aligned} \tag{255}$$

Consequently,

$$T'(\theta_{\max}) \approx -1.0219549. \tag{256}$$

The maxima have therefore crossed the multiplier -1 and are no longer attracting.

The phase-wide numerical diagnostic also detects negative exact-map thickness increments. On a uniform grid of 5×10^5 points we obtain

$$\min_{\theta}\big(d(T(\theta)) - d(\theta)\big) \approx -6.7492 \times 10^{-3}. \tag{257}$$

The negative value is separated from zero at the displayed scale and provides numerical evidence for loss of global thickness monotonicity in the exact geometric return map once the -2 bound is crossed.

9.7 A numerically resolved stable period-two orbit

For the profile (253), numerical solution of the exact-map period-two equation resolves a nontrivial two-cycle.

Using the signed angular coordinate in $(-\pi, \pi]$, one point of the cycle is

$$\theta_1 = 0.4081206459\ldots, \tag{258}$$

and the second is

$$\theta_2 = -0.4081206459\ldots. \tag{259}$$

Equivalently, on $[0, 2\pi)$,

$$\theta_2 = 5.8750646613\ldots.$$

At the displayed decimal approximations, direct evaluation of the exact map gives the residual bounds

$$|T(\theta_1) - \theta_2| < 10^{-12}, \qquad |T(\theta_2) - \theta_1| < 10^{-12}, \tag{260}$$

while $\theta_1 \neq \theta_2$. These inequalities record the numerical root accuracy; they are not written as exact identities.

The thickness takes the same value at the two cycle points:

$$d(\theta_1) = d(\theta_2) = 1.4222366310\ldots. \tag{261}$$

The derivative of the exact circle map at the two points is numerically

$$T'(\theta_1) = T'(\theta_2) \approx -0.762088583. \tag{262}$$

Hence the multiplier of the second iterate is the single product

$$(T^2)'(\theta_1) = T'(\theta_2)T'(\theta_1) \approx 0.580779008. \tag{263}$$

The computed multiplier lies well inside the unit circle,

$$|(T^2)'(\theta_1)| \approx 0.580779 < 1,$$

so the numerically resolved two-cycle is locally attracting at the level of the exact-map linearization.

Because the thickness profile has period $2\pi/3$, the numerical solution has three symmetry-related copies, one associated with each of the three former attracting maxima.

This provides exact-map numerical evidence of periodic attraction in a regime where the return geometry remains globally real but the strict Lyapunov mechanism is no longer observed.

9.8 A representative orbit approaching the two-cycle

Starting from

$$\theta_0 = 0.5, \tag{264}$$

the exact map produces the signed iterates listed in Table 2 and plotted over thirty steps in Figure 2.

Table 2. Exact orbit for $d(\theta) = 1.3 + 0.36\cos(3\theta)$, starting from $\theta_0 = 0.5$. Angles are represented in $(-\pi, \pi]$.

k	θ_k	$d(\theta_k)$
0	0.500000	1.325465
1	−0.424432	1.405528
2	0.419648	1.410456
3	−0.416470	1.413717
4	0.414261	1.415978
5	−0.412682	1.417592
6	0.411532	1.418765
7	−0.410685	1.419628
8	0.410055	1.420270
9	−0.409583	1.420750

The signed coordinate alternates while approaching

$$\pm 0.4081206459\ldots.$$

The thickness along this particular trajectory increases toward the common cycle value

$$1.4222366310\ldots,$$

even though the thickness is no longer globally monotone over the entire circle.

Failure of the global Lyapunov inequality means that monotonicity is lost somewhere in phase space; it does not require every individual orbit to exhibit a thickness decrease.

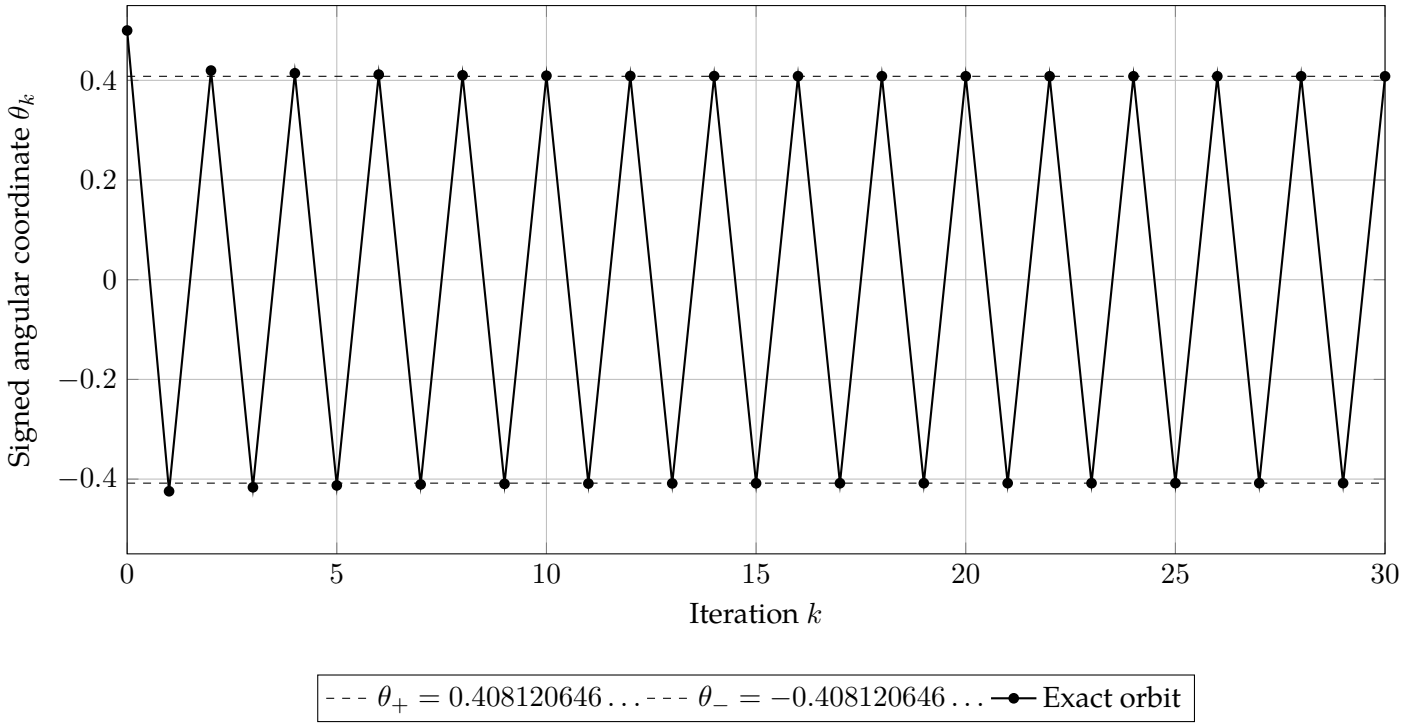

Figure 2. Exact return orbit for $d(\theta) = 1.3 + 0.36\cos(3\theta)$ with initial condition $\theta_0 = 0.5$. The signed angular iterates alternate between the two sides of the former fixed point $\theta = 0$ and approach the numerically resolved stable period-two cycle $\theta_\pm = \pm 0.408120646\ldots$. The iterates are generated from the exact geometric return map, not from its first-order approximation.

9.9 Reproducibility protocol

All iterations reported in this section are generated directly from the exact formulas (219)–(227).

For the phase-wide diagnostics, 5×10^5 equally spaced values of θ on $[0, 2\pi)$ were used. At each point we evaluated successively

$$d(\theta), \quad d'(\theta), \quad p(\theta), \quad \mathscr{R}(\theta), \quad \sigma(\theta), \quad \delta(\theta), \quad T(\theta),$$

and finally

$$d(T(\theta)) - d(\theta).$$

The period-two orbit in Section 9.7 was obtained by solving

$$T^2(\theta) - \theta = 0 \pmod{2\pi}, \tag{265}$$

while excluding fixed points of T. The root tolerance was 10^{-13}, and the displayed decimal representatives satisfy the residual bounds in (260).

For the symmetric cycle around $\theta = 0$, the equivalent signed equation

$$T(\theta) = -\theta \tag{266}$$

was used.

For the stability diagnostic we differentiate the exact formulas analytically rather than by finite differences. With $D = 1 + d$ one has

$$p' = \frac{d''D - (d')^2}{D^2},$$
$$\mathscr{R}' = -2(1+d)d'p^2 - 2d(2+d)pp',$$
$$\sigma' = \frac{\left(d' - \mathscr{R}'/(2\sqrt{\mathscr{R}})\right)(1+p^2) - 2pp'\left(1 + d - \sqrt{\mathscr{R}}\right)}{(1+p^2)^2}.$$

Writing

$$a = 1 + d - \sigma, \qquad b = \sigma p,$$

we have

$$a' = d' - \sigma', \qquad b' = \sigma' p + \sigma p'.$$

Since $a^2 + b^2 = 1$, differentiation of $\delta = \operatorname{atan2}(b, a)$ gives

$$T'(\theta) = 1 + a(\theta)b'(\theta) - b(\theta)a'(\theta). \tag{267}$$

Evaluation of (267) at the numerically resolved two-cycle yields

$$T'(\theta_1) = T'(\theta_2) \approx -0.762088583,$$
$$(T^2)'(\theta_1) \approx 0.580779008.$$

All computations were performed in radians. No iterate in the reported examples was generated from the first-order approximation to the return map.

9.10 Interpretation

The exact-map calculations distinguish three numerically observed dynamical regimes.

For the first subcritical profile, the sampled exact-map data show monotone thickness increase and convergence toward local maxima.

As the negative preconditioned curvature approaches -2, attracting maxima may be approached with alternating sign because their multipliers become negative while remaining inside the unit circle.

After the multiplier crosses -1, the fixed maximum loses local attraction. The example

$$d(\theta) = 1.3 + 0.36\cos(3\theta)$$

numerically resolves a stable period-two orbit of the exact geometric map while the first-intersection branch remains globally real.

The computation gives no indication of chaos; it shows that nontrivial periodic dynamics can arise once the hypotheses enforcing strict thickness ascent are violated. Whether further parameter variation produces higher-period cycles or more complicated invariant sets is a separate numerical and analytical question.

10 Discussion and Open Problems

The purpose of this paper has been to pass from the local geometric structure of the return map established in [2] to a genuinely global dynamical theory. The main mechanism is the interaction between the thickness gradient, the curvature-dependent preconditioner

$$B_c = d(c)\big(I - d(c)S_c\big)^{-1},$$

and the preconditioned Hessian

$$K_c = B_c^{1/2} H_c B_c^{1/2}.$$

Under a uniform local-return regime and a quantitative ascent condition, the thickness itself becomes a strict Lyapunov quantity:

$$d(F(c)) - d(c) \geq \gamma |\nabla_{\partial C} d(c)|^2.$$

This yields square summability of the thickness gradient, vanishing step size, convergence toward the critical set, and, under isolation of the critical points, convergence of every orbit to a single equilibrium.

The exact unit-circle computations of Section 9 also show that these hypotheses describe an actual dynamical regime and not only a proof device. Once the relevant spectral threshold is crossed, the numerical exact-map diagnostics show loss of thickness monotonicity while the first-intersection branch remains globally real, and a stable nontrivial period-two orbit is numerically resolved.

The remainder of this section discusses the scope of the theory and several questions that remain open.

10.1 The role of the preconditioned Hessian

A central structural feature of the analysis is that the same operator

$$K_c = B_c^{1/2} H_c B_c^{1/2} \tag{268}$$

appears at both the local and global levels.

At a critical point c_*, the exact derivative is

$$DF(c_*) = I + B_* H_*, \tag{269}$$

and the multipliers are

$$\lambda_j = 1 + \mu_j, \tag{270}$$

where the μ_j are the eigenvalues of K_*. Thus a negative preconditioned eigenvalue crosses the boundary of linear attraction precisely when

$$\mu_j = -2. \tag{271}$$

Globally, the second-order variation of the thickness has the form

$$d(F(c)) - d(c) = \left\langle z_c, \left(I + \frac{1}{2}K_c\right) z_c \right\rangle + \mathcal{E}(c), \tag{272}$$

where

$$z_c = B_c^{1/2}\nabla_{\partial C} d(c),\ |\mathcal{E}(c)| \leq \eta(|\nabla_{\partial C} d(c)|)|\nabla_{\partial C} d(c)|^2,$$

with $\eta(s) \to 0$ as $s \downarrow 0$. Accordingly, -2 is the spectral boundary at which the full quadratic form $I + \frac{1}{2}K_c$ ceases to be positive definite. This statement concerns the full spectrum; the dynamically sampled quadratic form along z_c may remain positive even when another eigendirection has crossed that boundary.

Both roles of -2 are thus produced by the return geometry itself.

The one-dimensional exact example of Section 9.6 makes this relation particularly transparent.

10.2 Directional versus spectral ascent conditions

The global theory was formulated using the directional condition

$$\left\langle z_c, \left(I + \frac{1}{2}K_c\right) z_c \right\rangle \geq \alpha_0 |z_c|^2, \tag{273}$$

where

$$z_c = B_c^{1/2} \nabla_{\partial C} d(c).$$

The stronger spectral condition

$$\lambda_{\min}(K_c) \geq -2 + \delta \tag{274}$$

was introduced only as a convenient sufficient criterion.

The return dynamics samples the quadratic form only in the dynamically selected direction z_c. There may therefore exist geometries for which

$$\lambda_{\min}(K_c) < -2$$

in a direction never sufficiently aligned with z_c, while the actual return dynamics still possesses a strict Lyapunov structure.

Determining the optimal condition for global ascent is therefore a more subtle problem than bounding the full spectrum of K_c.

Open Problem 10.1 (Sharp global ascent criterion)**.** *Characterize the largest class of geometries for which*

$$d(F(c)) > d(c) \qquad \text{whenever } \nabla_{\partial C} d(c) \neq 0. \tag{275}$$

In particular, determine whether the directional quadratic condition (273)*, combined with an appropriate exact control of the nonlinear return geometry, can replace the stronger uniform spectral bound* (274)*.*

10.3 How much smallness is really necessary?

The uniform global one-step estimate was derived under the small-slope condition

$$\|w\|_{L^\infty(\partial C)} \leq \varepsilon_0, \; w_c = \big(I - d(c) S_c\big)^{-1} \nabla_{\partial C} d(c). \tag{276}$$

Its role was geometric: it guarantees that every return point $F(c)$ lies in the uniform normal-graph neighborhood of its starting point, allowing the exact closure relation to be converted into a uniform quadratic remainder estimate.

The condition is sufficient, but no optimality is claimed. It may be possible to obtain global control without requiring the entire return to remain inside one normal coordinate patch centered at c.

Indeed, the exact return map exists under considerably broader geometric conditions than those used to prove the perturbative one-step estimate. This is already visible in the circle experiments, where the exact map remains real and single valued even after the strict monotonicity regime has been lost.

Open Problem 10.2 (Beyond the small-slope regime)**.** *Determine whether the exact return geometry admits a nonperturbative estimate for*

$$d(F(c)) - d(c)$$

that does not require the uniform small-slope hypothesis (276)*.*

A particularly interesting question is whether the closure equation for the convex core can be combined with global convexity to produce an exact monotonicity criterion expressed directly in terms of d, S, and the first-return geometry.

10.4 The -2 threshold and bifurcation

The exact unit-circle family

$$d(\theta) = d_0 + \varepsilon \cos(m\theta)$$

provides a tractable model for studying the loss of monotonicity.

At a thickness maximum, the preconditioned Hessian is

$$\mu = -m^2 \varepsilon \frac{d_0 + \varepsilon}{1 + d_0 + \varepsilon}, \tag{277}$$

and the fixed-point multiplier is

$$\lambda = 1 + \mu. \tag{278}$$

Thus

$$\mu = -2$$

is exactly the parameter value at which

$$\lambda = -1.$$

Section 9.7 studies an exact-map example with

$$\mu < -2$$

for which the former attracting maximum is unstable and a stable period-two orbit is numerically resolved. This suggests that the -2 threshold is a genuine bifurcation boundary for at least some one-parameter families of return geometries.

The numerical evidence, however, does not by itself establish the type of bifurcation.

Open Problem 10.3 (Local flip bifurcation). *Consider a smooth one-parameter family of admissible thickness functions*

$$d_\xi$$

for which a nondegenerate maximum persists as a fixed point $c_*(\xi)$ and one multiplier crosses -1 transversely.

Determine geometric nondegeneracy conditions under which the return map undergoes a genuine period-doubling, or flip, bifurcation [18] at the parameter value satisfying

$$\mu(\xi_*) = -2.$$

In particular, derive the relevant normal-form coefficient directly from the geometry of C and the derivatives of the thickness function.

Such a result would provide an analytical explanation for the period-two orbit found in the exact circle experiment.

10.5 Dynamics beyond the first loss of monotonicity

The numerically resolved stable period-two orbit indicates that once the strict Lyapunov regime fails, the return dynamics need no longer converge to fixed points. It does not imply that more complicated dynamics must occur.

A first-order surrogate map is not sufficient for conclusions about the exact return dynamics beyond the monotone regime. The appropriate object for further study is the exact first-return map itself.

Open Problem 10.4 (Higher-period dynamics). *Within a smooth parameter family for which the exact return remains well defined, determine whether stable cycles of periods*

$$p \geq 3$$

can occur after the loss of the global ascent condition.

For the unit-circle cosine family, construct the bifurcation diagram of the exact map

$$T(\theta) = \theta + \delta(\theta) \pmod{2\pi}$$

as (d_0, ε, m) vary, using the exact first-intersection branch throughout.

Open Problem 10.5 (Complicated recurrent dynamics). *Determine whether there exist admissible domains in the class $\mathcal{O}_C$ for which the exact return map possesses invariant sets with genuinely nonperiodic recurrent dynamics.*

Any claim of chaotic behavior should be based on the exact return map and supported by appropriate dynamical evidence, such as positive Lyapunov exponents, entropy estimates, symbolic dynamics, or rigorously verified transverse homoclinic structure.

10.6 Nonisolated critical sets

The isolation assumption on $\mathrm{Crit}(d)$ enters only in the final step of the global convergence proof. Without it, the Lyapunov theory still yields

$$\mathrm{dist}\big(c_k, \mathrm{Crit}(d)\big) \longrightarrow 0 \tag{279}$$

and

$$\omega(c_0) \subset \mathrm{Crit}(d) \cap d^{-1}(d_\infty), \tag{280}$$

but convergence to one point need not follow from the present argument.

Open Problem 10.6 (Critical manifolds and degenerate equilibria). *Suppose that $\mathrm{Crit}(d)$ contains a smooth critical submanifold or a more general compact connected component.*

Under what additional analytic or geometric assumptions does every return orbit still converge to a single point of that component?

One possible direction is to seek a gradient inequality for the thickness near the critical set that strengthens square summability of the gradient to a finite-length property of the orbit.

This question is distinct from the Morse-theoretic analysis of isolated nondegenerate critical points.

10.7 Basin boundaries and invariant manifolds

Section 8 established only the rigorous inclusion

$$\partial\mathcal{B}(a) \subset \bigsqcup_{q \in \mathcal{N}} \mathcal{C}(q) \tag{281}$$

for an attracting equilibrium a.

A stronger description in terms of stable manifolds of saddle points requires additional dynamical hypotheses and cannot be inferred from the Lyapunov structure alone.

Open Problem 10.7 (Separatrix structure). *Assume that all critical points are hyperbolic and that the return map is locally invertible at the relevant equilibria.*

Determine additional transversality conditions under which the boundaries of attraction basins are unions of stable manifolds of saddle points.

More generally, identify conditions under which the resulting invariant-manifold structure is Morse–Smale.

This issue is especially relevant in dimensions greater than one, where different stable and unstable dimensions can interact in ways that have no analogue for the circle map.

10.8 Higher-dimensional return dynamics

The analytical results of Sections 3–8 are dimension independent. The exact circle computations, however, probe only a one-dimensional phase space.

For

$$\dim \partial C \geq 2,$$

the preconditioning operator B_c becomes anisotropic and the preconditioned Hessian K_c may possess several competing spectral directions. Consequently, loss of the ascent condition can occur in only part of the tangent space.

Open Problem 10.8 (Anisotropic loss of stability). *Study parameter families for which one or several eigenvalues of K_* cross -2 while the remaining eigenvalues stay inside $(-2, 0)$.*

Determine how the geometry of the corresponding eigenspaces influences the bifurcation of the return dynamics and whether the first loss of stability produces periodic, quasiperiodic, or higher-dimensional invariant structures.

Here the curvature of the convex core enters essentially: even for a fixed Hessian H_c, changing the principal curvatures modifies the operator B_c and therefore changes the relevant preconditioned spectrum.

10.9 Robustness under perturbation

The global ascent regime is expressed through strict inequalities. This suggests a degree of robustness under sufficiently small smooth perturbations of the geometry.

If, for example,

$$\lambda_{\min}(K_c) \geq -2 + \delta$$

with a fixed margin $\delta > 0$, then sufficiently small perturbations of d and of the geometry of ∂C preserve the corresponding spectral inequality.

A complete perturbation theory must nevertheless account simultaneously for the radial map, the reciprocal first-hit map, the return transversality constant, and the uniform local-return threshold.

Open Problem 10.9 (Structural robustness). *Quantify the stability of the global convergence regime under perturbations of the pair (C, Ω).*

In particular, determine explicit geometric norms and perturbation bounds that preserve:

1. *the single-valued return construction;*
2. *uniform return transversality;*
3. *the global one-step estimate;*
4. *strict thickness ascent;*
5. *convergence to isolated critical points.*

10.10 Continuous-time interpretation

The leading return displacement

$$F(c) - c \approx B_c \nabla_{\partial C} d(c)$$

has the formal appearance of one step of a curvature-preconditioned gradient-ascent process.

The present paper does not identify the discrete return map with a time discretization of a continuous flow. Such an interpretation would require an explicit small-step scaling and a consistency analysis over finite time intervals. This distinction was already important in the foundational analysis [2].

A natural candidate continuous dynamics is

$$\dot{c} = B_c \nabla_{\partial C} d(c), \tag{282}$$

for which

$$\frac{d}{dt} d(c(t)) = \left\langle \nabla_{\partial C} d(c(t)), B_{c(t)} \nabla_{\partial C} d(c(t)) \right\rangle \geq 0. \tag{283}$$

Open Problem 10.10 (Scaled continuous-time limit). *Construct a geometrically natural parameter family for which the return displacement tends uniformly to zero and prove, after an appropriate rescaling of discrete time, convergence of the return orbits to solutions of (282) or to the corresponding limiting preconditioned flow.*

10.11 Perspective

The results identify the following implication for the return dynamics:

uniform return control
+ preconditioned ascent
+ isolated critical points
$\Downarrow$
strict Lyapunov structure
+ global convergence
+ absence of nontrivial recurrence.

Within this regime, the thickness landscape organizes the asymptotic dynamics, but its action is mediated by the curvature of the convex core through B_c. Outside this regime, the geometry can generate qualitatively different behavior even while the return map remains regular and single valued.

The numerically resolved period-two orbit of the exact unit-circle map marks the first such transition exhibited here. It shows that the boundary between convergent and nonconvergent dynamics is itself a geometric object worthy of study.

The resulting picture is therefore not one of an abstract gradient algorithm imposed on the boundary. The discrete dynamics is produced by the nested geometry itself, and both its convergent regime and its possible bifurcations are encoded by the interaction between thickness variation, curvature, and normal return geometry.

11 Conclusion

The global behavior of the return map in the class $\mathcal{O}_C$ can be controlled by properties of the core geometry and its thickness function. Under uniform transversality and small-slope assumptions, the return displacement admits a uniform curvature-preconditioned expansion whose tangential remainder is cubic. The resulting second-order thickness formula gives sufficient conditions for strict ascent, a Lyapunov inequality, and convergence of every orbit to a single critical point when the critical set is isolated. These conclusions apply standard discrete-dynamical arguments to a geometrically generated map; their distinct contribution is the verification of those arguments through explicit return geometry. Exact unit-circle computations also exhibit loss of monotonicity and a numerically resolved stable period-two orbit outside the sufficient ascent regime. A complete bifurcation theory and a treatment of nonisolated critical sets remain open.

Data Availability Statement

No external datasets were used in this study. The numerical values reported in Section 9 can be reproduced directly from the formulas and parameters provided in the manuscript.

Funding

This work was supported without any funding.

Conflicts of Interest

Mohamed El Morsalani is affiliated with the QWave Consult, Ostfildern, Germany. The authors declare that this affiliation had no influence on the study design, data collection, analysis, interpretation, or the decision to publish, and that no other competing interests exist.

AI Use Statement

The authors declare that ChatGPT-6 was used for language editing and translation of the manuscript. The authors have carefully reviewed, revised, and verified the AI-assisted output and take full responsibility for the content of the manuscript.

Ethical Approval and Consent to Participate

Not applicable.

References

[1] Barkatou, M. (2002). Some geometric properties for a class of non-Lipschitz domains. *New York Journal of Mathematics, 8*, 189-213. https://nyjm.albany.edu/j/2002/8-13.html

[2] Barkatou, M., & El Morsalani, M. (2026). The return map in the class $\mathcal{O}_C$: Geometry, dynamics, and thickness regularity. *Journal of Nonlinear Dynamics and Applications*, 2(3), 192-216. [CrossRef]

[3] Schulz, V. H. (2014). A Riemannian view on shape optimization. *Foundations of Computational Mathematics, 14*(3), 483-501. [CrossRef]

[4] Welker, K. (2021). Suitable spaces for shape optimization. *Applied Mathematics & Optimization, 84*(Suppl. 1), S869-S902. [CrossRef]

[5] Plotnikov, P. I., & Sokolowski, J. (2023). Geometric aspects of shape optimization. *The Journal of Geometric Analysis, 33*(7), 206. [CrossRef]

[6] Huang, W., & Wei, K. (2022). Riemannian proximal gradient methods. *Mathematical Programming, 194*(1-2), 371-413. [CrossRef]

[7] Huang, W., & Wei, K. (2023). An inexact Riemannian proximal gradient method. *Computational Optimization and Applications, 85*(1), 1-32. [CrossRef]

[8] Attouch, H., Bolte, J., & Svaiter, B. F. (2013). Convergence of descent methods for semi-algebraic and tame problems: proximal algorithms, forward-backward splitting, and regularized Gauss-Seidel methods. *Mathematical Programming, 137*(1-2), 91-129. [CrossRef]

[9] Bento, G. C., Mordukhovich, B. S., Mota, T. S., & Nesterov, Y. (2025). Convergence of descent optimization algorithms under

Polyak-Łojasiewicz-Kurdyka conditions. *Journal of Optimization Theory and Applications, 207*(3), 41. [CrossRef]

[10] Kurdyka, K. (1998). On gradients of functions definable in o-minimal structures. *Annales de l'Institut Fourier, 48*(3), 769-783. [CrossRef]

[11] Absil, P.-A., Mahony, R., & Sepulchre, R. (2008). *Optimization Algorithms on Matrix Manifolds*. Princeton University Press. [CrossRef]

[12] Luchnikov, I. A., Krechetov, M. E., & Filippov, S. N. (2021). Riemannian geometry and automatic differentiation for optimization problems of quantum physics and quantum technologies. *New Journal of Physics, 23*(7), 073006. [CrossRef]

[13] Absil, P. A., Mahony, R., & Andrews, B. (2005). Convergence of the iterates of descent methods for analytic cost functions. *SIAM Journal on Optimization, 16*(2), 531-547. [CrossRef]

[14] Katok, A., & Hasselblatt, B. (1995). *Introduction to the Modern Theory of Dynamical Systems* (Encyclopedia of Mathematics and its Applications, Vol. 54). Cambridge University Press. [CrossRef]

[15] Palis, J., Jr., & de Melo, W. (1982). *Geometric Theory of Dynamical Systems: An Introduction*. Springer-Verlag. [CrossRef]

[16] Lee, J. D., Simchowitz, M., Jordan, M. I., & Recht, B. (2016). Gradient descent only converges to minimizers. In *Proceedings of the 29th Annual Conference on Learning Theory* (PMLR, Vol. 49, pp. 1246-1257). https://proceedings.mlr.press/v49/lee16.html

[17] Smale, S. (1961). On gradient dynamical systems. *Annals of Mathematics, 74*(1), 199-206. [CrossRef]

[18] Guckenheimer, J., & Holmes, P. (1983). *Nonlinear Oscillations, Dynamical Systems, and Bifurcations of Vector Fields* (Applied Mathematical Sciences, Vol. 42). Springer-Verlag. [CrossRef]

Mohamed El Morsalani is a mathematician, researcher, and quantum technologies consultant at QWave Consult in Ostfildern, Germany. He holds a PhD in mathematics and has more than two decades of professional experience in quantitative finance, risk analysis, and advanced technologies. His mathematical research focuses on geometric analysis and dynamical systems, particularly the geometric and dynamical analysis of return maps in structured classes of domains. In parallel, his research in quantum technologies addresses quantum cryptography, post-quantum cryptography, open quantum dynamics, and the geometric foundations of quantum information, including mixed-state geometry and holonomy-based secrecy frameworks. His work is driven by a broader interest in uncovering and analyzing hidden geometric and dynamical structures across both classical and quantum systems. (Email: mohamed.elmorsalani@qwave-consult.eu)

Mohammed Barkatou is a mathematician at Chouaïb Doukkali University in Morocco. He holds a Ph.D. in Mathematics and Applications from the University of Franche-Comté (France). His research focuses on shape optimization, free boundary problems, calculus of variations, and discrete optimization. He has supervised 5 doctoral theses. (Email: barkatou.m@ucd.ac.ma)